Title: Parallel genome-scale CRISPR screens distinguish pluripotency and self-renewal

Authors:

Bess P. Rosen[1,2], Qing V. Li[1,3,4], Hyunwoo Cho[1], Dingyu Liu[1,3], Dapeng Yang[1], Sarah Graff[5], Jielin Yan[1,3], Renhe Luo[1,3], Nipun Verma[1,6], Jeyaram R. Damodaran[1], Michael A. Beer[7], Simone Sidoli[5], Danwei Huangfu[1,8,*]

Affiliations:

[1] Developmental Biology Program, Sloan Kettering Institute; 1275 York Avenue, New York, NY 10065, USA.

[2] Weill Cornell Graduate School of Medical Sciences, Weill Cornell Medicine; 1300 York Avenue, New York, NY 10065, USA.

[3] Louis V. Gerstner Jr. Graduate School of Biomedical Sciences, Memorial Sloan Kettering Cancer Center, 1275 York Avenue, New York, NY 10065, USA.

[4] Present address: Tessera Therapeutics, 55 Cambridge Parkway, Cambridge, MA 02139, USA.

[5] Department of Biochemistry, Albert Einstein College of Medicine, 1300 Morris Park Avenue, Bronx, NY 10461, USA.

[6] Present address: Department of Therapeutic Radiology, Yale School of Medicine, 333 Cedar Street, New Haven, CT 06510, USA.

[7]Department of Biomedical Engineering and McKusick-Nathans Department of Genetic Medicine, Johns Hopkins University; Baltimore, MD 21218, USA.

[8]Lead contact

* Correspondence: Huangfud@mskcc.org (DH)

Summary

Pluripotent stem cells are defined by both the ability to unlimitedly self-renew and differentiate to any somatic cell lineage, but understanding the mechanisms that control stem cell fitness versus the pluripotent cell identity is challenging. We performed four parallel genome-scale CRISPR-Cas9 screens to investigate the interplay between these two aspects of pluripotency. Our comparative analyses led to the discovery of genes with distinct roles in pluripotency regulation, including many mitochondrial and metabolism regulators crucial for stem cell fitness, and chromatin regulators that control stem cell identity. We further discovered a core set of factors that control both stem cell fitness and pluripotency identity, including an interconnected network of chromatin factors that safeguard pluripotency. Our unbiased and systematic screening and comparative analyses disentangle two interconnected aspects of pluripotency, provide rich datasets for exploring pluripotent cell identity versus self-renewal, and offer a valuable model for categorizing gene function in broad biological contexts.

Keywords:

Human embryonic stem cells (hESCs), pluripotency, self-renewal, cell fitness, genome-scale CRISPR-Cas9 genetic screening, differentiation, functional genomics, human pluripotent stem cells, OTUD5

Introduction

Human pluripotent stem cells (hPSCs), which include embryonic stem cells (hESCs) and induced pluripotent stem cells (hiPSCs), have two interconnected properties: pluripotency, the ability to differentiate into all somatic cells, and self-renewal, the ability to proliferate while maintaining pluripotency. These properties make hPSCs invaluable for biomedical research and therapeutic applications, leading many researchers to study pluripotency regulation. While there are commonalities in the mechanisms governing pluripotent identity and self-renewal, evidence also suggests the involvement of distinct regulatory pathways. The transcription factors (TFs) OCT4 (POU5F1), NANOG, and SOX2 are well-established master regulators of pluripotent identity [1–5] that cooperatively regulate one another as well as a large set of downstream genes in hPSCs [6,7]. However, the downregulation of these master regulators during hPSC differentiation is accompanied by decreased susceptibility to apoptosis, with OCT4 depletion in some contexts even imparting a competitive advantage in hESC self-renewal [8,9]. In other words, these positive regulators of pluripotency are not always positive regulators of self-renewal. Recent advances in CRISPR-Cas9 genome editing have enabled the use of large-scale loss-of-function screens to interrogate self-renewal through assaying cell survival and proliferation [9–13]. Defining the hPSC essentialome through unbiased self-renewal screens not only provides valuable information for more effective use of hESCs in studies of human development, disease, and clinical translation, but also expands our knowledge of pluripotency regulation in human development [14]. Somewhat unexpectedly, previous screens for hPSC self-renewal did not rank OCT4, NANOG, and SOX2 among the top pro-self-renewal hits, indicating that these pluripotency factors may not be the strongest drivers of self-renewal. By extension, self-renewal screens may fail to identify other key pluripotency regulators that have weak or modest involvement in self-renewal. Therefore, new assays are needed to identify genes that safeguard pluripotent identity.

We reasoned that pluripotency in development is transient and quickly transitions into the three germ layers, thus a more effective approach to unraveling the regulation of pluripotency should investigate the dissolution of pluripotent cell identity during hESC differentiation. We applied guided neuroectoderm (NE) and definitive endoderm (DE) differentiation protocols [15,16] to mimic the pluripotent cells in the epiblast making the first lineage commitment to differentiate into ectoderm or mesendoderm lineages at the onset of gastrulation. These lineage transitions involve the loss of the pluripotent identity and the gain of a new lineage identity. Distinct from previous differentiation screens that inspected the acquisition of a new cell fate during directed differentiation [9,17], we designed our pluripotency screens to examine the loss of pluripotency using a knockin fluorescent reporter for *OCT4* expression. We identified many shared hits between our NE and DE pluripotency screens, pointing to a common program orchestrating the dissolution of pluripotency independent of differentiation context. Furthermore, comparison of our pluripotency screens to previous differentiation screens [9,17] highlights distinct forces that drive cell state transitions: those that pull towards a new state, and those that push away from the old state.

Our pluripotency screens conducted during dynamic cell state transitions discovered genes that control pluripotent identity independent of differentiation context. We further investigated the regulation of pluripotency during differentiation in comparison to results from self-renewal screens [11–13]. For better matched comparisons, we conducted our own self-renewal screens, and categorized hits into gene modules with distinct or similar impacts on pluripotent identity or self-renewal. Ontological analyses of screen hits suggest that self-renewal screens are more effective at uncovering genes related to stem cell fitness, such as mitochondrial components and cell cycle regulators, while our pluripotency screens are more effective at identifying regulators of the stem cell identity, many of which are chromatin factors. Defining modules containing positive regulators of both pluripotency and self-renewal allowed us to expand the core pluripotency network involving OCT4, NANOG and SOX2 through the

100 identification of new hits such as the deubiquitinase OTUD5. Comparison of our multiple parallel CRISPR screens provides an effective gene characterization and discovery model that enabled us to disentangle two interconnected aspects of pluripotency: pluripotent cell identity versus stem cell fitness.

105 **Genome-scale screens for regulators of pluripotency**

To discover regulators of pluripotency during differentiation, we used the expression of core pluripotency and early embryogenesis regulator OCT4 [1,2,18] as a readout for the pluripotent state. Using our established selection free knock-in strategy [19], we generated an *OCT4*-GFP reporter in the H1 iCas9 hESC line, which expresses Cas9 upon doxycycline treatment [20]
110 (**Figure S1A,B**). *OCT4*-GFP decreased upon NE and DE differentiation (**Figure S1C,D**), mirroring the downregulation of *OCT4* expression during the dissolution of the pluripotency network. We next conducted parallel screens in NE and DE differentiation conditions to distinguish whether the regulation of pluripotency was largely differentiation context dependent, or if a shared group of regulators might control the dissolution of pluripotency regardless of
115 differentiation context. Using a pooled screening strategy [17,21,22], we infected H1 OCT4$^{GFP/+}$ iCas9 hESCs with a genome-scale CRISPR library [23] (**Figure 1A**). OCT4-GFP^{hi} and OCT4-GFP^{lo} were isolated by fluorescence-activated cell sorting (FACS) on day 1.5 of NE (**Figure S2A,B**) and day 2.5 of DE (**Figure S2C,D**) differentiations, matching the timepoints when *OCT4*-GFP was rapidly downregulated (**Figure S1C**). The MAGeCK robust ranking aggregation
120 (RRA) algorithm [24] was used to identify genes that promote or inhibit pluripotency based on relative gRNA enrichment in the OCT4-GFP^{lo} or OCT4-GFP^{hi} population, respectively. We selected the top 150 genes in each category as hits based on RRA scores. To assist comparisons between the NE and DE screens, we also calculated a “pluripotency score” for each gene in each screen equal to log10(RRA score OCT4-GFP^{hi} enrichment) – log10(RRA
125 score OCT4-GFP^{lo} enrichment) (**Table S1**). Strikingly, despite the screens being performed in

different differentiation contexts, the results of the NE and DE screens were moderately correlated (Pearson correlation coefficient $r = 0.56$), with a significant number of overlapping hits: 40 hits that promote pluripotency (pro-pluripotency) and 39 hits that inhibit pluripotency (anti-pluripotency) (**Figure 1B,C**). Gene set enrichment analysis (GSEA) revealed significant enrichment (Normalized Enrichment Score, NES, greater than 3.2) of pro-pluripotency hits from one screen in genes ranked by the pluripotency scores in the other screen; and strong negative enrichment (NES < –3.2) of anti-pluripotency hits (**Figure 1D**). These results suggest a high degree of concordance between NE and DE screens, and the presence of common mechanisms controlling the loss of pluripotency regardless of the external differentiation cues.

Some of the anti-pluripotency hits are also known positive regulators of differentiation. For instance, *SOX11* is a neural regulator [25], and *FOXH1*, *SMAD2*, *SMAD4*, and *EOMES* regulate DE specification in mice and humans [17,26–29]. Therefore, we compared pro- and anti-pluripotency hits found in our screens to the anti- and pro-differentiation hits identified from previous screens interrogating the specification of SOX17^{+} DE and EPCAM^{-}/NCAM^{+} NE fates [9,17] (**Figure S3A,B**). A small number of genes were identified as both pro-pluripotency and anti-differentiation, or both anti-pluripotency and pro-differentiation, supporting the interconnectivity of the acquisition of the new cell identity and the dissolution of the pluripotent state (**Figure S3C**). However, most of the pluripotency hits were not identified in previous differentiation screens. For a better matched comparison, we compared the DE pluripotency screen with our previous DE differentiation screen [17] conducted under closely matched differentiation and screening conditions, and conducted systemic analysis of overlapping and non-overlapping hits using STRING (v11.5) [30] and GO term enrichment [31] (**Figure S3D,E**). The results showed that top hits unique to the DE differentiation screen included regulators of developmental signaling pathways, and Golgi-associated transport and processing. In contrast, top hits unique to the pluripotency screen were chromatin modifiers and transcriptional regulators, and genes involved in RNA processing. The different hits identified from screens performed in the same

differentiation context suggests that the gene network regulating the pull of differentiation can be decoupled from the push of pluripotency loss.

With the aim of identifying specific regulators of pluripotency, rather than differentiation, we selected 19 genes not known to be regulators of lineage specification for further validation: 16 genes identified as pro-pluripotency in at least one screen, and 3 genes identified as anti-pluripotency. Lentiviral vectors expressing gene-specific gRNAs were used to infect H1 OCT4$^{GFP/+}$ iCas9 hESCs followed by individual differentiation assays. Using *OCT4*-GFP mean fluorescent intensity (MFI) relative to non-targeting controls as measured by flow cytometry, we validated 15 and 16 hits in NE and DE differentiation, respectively (**Figure 1E,F, Figure S4**). Validation phenotypes correlated strongly with pluripotency scores in each screen (**Figure 1G,H**). Hits validated in both NE and DE contexts included genes not previously connected to the regulation of pluripotency, such as *OTUD5*, *ZNF423*, *SLTM,* and *UBA6*. Validation results in NE and DE contexts were also well correlated (**Figure S4E**), and several genes (e.g., *RFWD2*, *SOX2*, *EP300*, and *SLTM*) identified among the top 150 hits in only one screen were validated in both NE and DE contexts. Our screening and validation studies reveal the existence of a common program that controls the dissolution of pluripotency across different differentiation contexts, and this program is distinct from those that govern lineage specification.

Parallel Screens reveal distinct regulation of pluripotency and self-renewal

To compare the regulation of pluripotent identity in differentiation contexts to regulation of self-renewal in maintenance conditions, we conducted two additional pooled genome-scale screens. The first screen was performed in the chemically defined serum-free E8 media [32] containing FGF2 and TGFβ, both essential for hESC maintenance (**Figure 2A, Figure S5A**); and the second screen used a “challenge” condition wherein cells were exposed to E6 media (similar to E8 but without FGF2 and TGFβ) for five days before returning the cells back to the standard E8 condition for one passage (**Figure 2A, Figure S5B**). We used the MAGeCK RRA

algorithm [24] to identify genes that promote or inhibit self-renewal based on relative gRNA enrichment in Day 0 or Day 10, respectively, and selected the top 150 genes in each category as hits based on RRA scores. To assist comparisons between the E8 and E6 screens, we also calculated a "self-renewal score" for each gene equal to log10(RRA score Day 10 enrichment) – log10(RRA score Day 0 enrichment) (**Table S1**). There were large numbers of overlapping pro-self-renewal (85) and anti-self-renewal (24) hits between the E8 and E6 screens (**Figure 2B, Figure S5C**), and GSEA analysis revealed strong enrichment of hits identified from one screen in genes ranked by the self-renewal scores in the other screen (**Figure S5D**). The smaller number of overlapping anti-self-renewal hits is likely because the E8 condition is already optimized for self-renewal, whereas the E6 challenge condition allows better identification of anti-self-renewal hits, as also supported by the greater range of negative self-renewal scores observed in the E6 as compared to the E8 screen. Nevertheless, we still identified many shared anti-self-renewal hits, including known negative regulators of hESC self-renewal such as *TP53* and *PMAIP1,* while the E6 screen also identified additional hits, including *PTEN*, *TSC1*, and *TSC2* which were identified as anti-self-renewal genes in a previous CRISPR screen [11].

We assessed the degrees of correlation between hits in all four screens based on self-renewal and pluripotency scores. Hits from the E8 and E6 screens showed a strong correlation in self-renewal scores (Pearson correlation coefficient $r = 0.82$), and hits from the DE and NE screens also showed correlated pluripotency scores as described. In contrast, we did not observe any positive correlation between self-renewal and pluripotency scores across the two screening types (**Figure S5E**). Consistent with the correlation analysis, we found that self-renewal screening hits were not highly ranked in the pluripotency screens (**Figure 2C**), while pluripotency screen hits (**Figure 2D**) were not highly ranked in the self-renewal screens (**Figure 2E**). Indeed, very few genes were identified as promoting both pluripotency and self-renewal or, conversely, inhibiting both pluripotency and self-renewal (**Figure 2F**). We expanded the comparison to include the top 150 pro-self-renewal hits from previous self-renewal screens in a

variety of hESC maintenance conditions [11–13] (**Table S2**) as gene sets for GSEA analysis. There
205 was a high degree of enrichment of hits from these previous self-renewal screens in the E8 and E6 screen results (NES ranging from 2.46 to 3.97) but not in the DE and NE pluripotency screen results (**Figure 2G, Figure S5F**). This contrast between the two types of screens demonstrates the existence of distinct mechanisms that regulate pluripotency or self-renewal, and emphasizes the need for direct interrogation of the pluripotent cell identity during dynamic lineage transitions.

210 Analysis with STRING [30] showed distinct protein complexes were discovered in pluripotency and self-renewal top hits (**Figure 2H**). The NE and DE screens identified many chromatin regulators. Some of these have been implicated in pluripotency regulation such as the Spt-ADA-Gfn5 (SAGA) complex [33,34], the transcriptional regulating mediator complex [35], the chromatin remodeling INO80 complex [36], and the ATP dependent nucleosome remodeling
215 BRG1-associated factor (BAF) complex (also known as the SWI/SNF complex) [37–40]. In contrast, complexes identified as pro-self-renewal in the E8 and E6 screens included mitochondrial components and regulators of DNA-repair and tRNA metabolism, consistent with the findings of previous self-renewal screens [11,12]. We performed Reactome pathway analysis [41] on hits from each screen, then ranked sets by median absolute $\log_2$(fold change of screening enrichment)
220 (LFC) of all hits in set (**Figure S6A**). Members of the “chromatin organization”, “HATs acetylate histones”, and related Reactome sets had a high median |LFC| in NE and DE pluripotency screens, whereas genes from the “mitochondrial translation”, “tRNA aminoacylation”, and related sets had a high median |LFC| in E8 and E6 self-renewal screens (**Figure S6A**). The overrepresentation of mitochondrial components and tRNA processing genes in pro-self-
225 renewal hits, as revealed by both STRING and Reactome analyses, suggests that the self-renewal screens preferentially capture genes required for cell fitness. Supporting this notion, >40% of pro-self-renewal hits in our E8 and E6 screens are categorized as common essential genes based on integrated screening results from hundreds of cancer cell lines [42–46] (**Figure 2I, Figure S6B, Table S2**). Similarly, a high proportion of common essential genes was

230 also found in previous hESC self-renewal screens [11–13] (**Figure S6C**). In contrast, fewer than 10 pro-pluripotency hits from the NE or DE screens overlapped with common essential genes. Together, these results indicate that the self-renewal screens predominantly identify regulators of stem cell fitness, while our pluripotency screens in differentiation contexts mainly uncover regulators of the stem cell identity. In addition, chromatin modulation plays a key role in
235 regulating pluripotency during cell fate transition.

Comparative analysis uncovers distinct gene modules in pluripotency and self-renewal

To dissect gene modules with distinct roles regulating pluripotency and self-renewal, we performed unbiased hierarchical clustering of all pro-pluripotency and pro-self-renewal hits by
240 the column scaled LFC in all 4 screens (**Figure 3A, Table S3**). This approach revealed 8 gene modules that exhibited distinct patterns in their pluripotency and self-renewal scores (**Figure 3B**). Reassuringly, analysis of individual modules by STRING showed association between proteins corresponding to genes in the same module, suggesting that our clustering method based on findings from genetic screening data is effective for grouping hits with similar
245 biochemical functions (**Figure S7**). Many of these modules were primarily enriched for either pro-pluripotency or pro-self-renewal hits, and reflected broader screen findings regarding the regulation of pluripotent identity and self-renewal. For example, module 1, 4 and 5, which consisted largely of pro-self-renewal hits, were enriched for regulators of mitochondrial translation, mitochondrial respiration, or both (**Figure S7**). This is consistent with our and
250 previous findings connecting mitochondrial regulation with essentiality in pluripotency [11]. In comparison, module 3 and 2, both containing pro-pluripotency hits, were enriched for genes involved in the signaling pathways regulating pluripotency including WNT, TGFβ, and Hippo signaling, and a host of developmental TFs, respectively. Module 6 was notable for its enrichment of genes that were identified as strongly pro-pluripotency but anti-self-renewal,
255 which included many members of the SAGA histone acetyltransferase and core complex, the

mediator complex, and the recently identified non-canonical (ncBAF) complex [47,48] (**Figure 3C**). Overall, STRING analyses revealed great interconnectivity between components within each module. The gene relationships identified in these modules demonstrate both the utility of clustering multi-context screening data to identify distinct regulatory programs, and the potential for inferring the biochemical functions of uncharacterized genes.

One module, module 8, was noteworthy in that it was highly enriched for genes that were highly ranked as both pro-pluripotency (in NE, DE, or both) and pro-self-renewal (in E8, E6 or both). Module 8 included all 3 core pluripotency factors OCT4, NANOG, and SOX2, as well as PRDM14, a TF which is essential to the maintenance of human pluripotency [36,49,50] (**Figure 3C**). There were also chromatin remodelers associated with pluripotency including coactivator EP300 [51], Polycomb complex member EED [52], mediator complex members MED19 and MED25 [35], and BAF ATPase SMARCA4 [37–40,47,48,53]. Notably, analysis by STRING showed a great degree of functional protein association within this module (**Figure 3C**). The large number of module 8 members involved with chromatin accessibility and transcriptional control of pluripotency suggests a similar role for other hits in this module such as OTUD5 and RUNX1T1 that were not previously connected to pluripotency.

OTUD5 and *TADA2B* are pro-pluripotency genes with opposing roles in self-renewal

Module 6 and module 8 from our comparative analysis both captured genes with high pluripotency scores, yet they were differentiated by enrichment with genes with opposing effects on self-renewal (**Figure 3B,C**). For further investigation, we chose two archetypical examples of screen hits from each of these modules: *OTUD5* (in module 6) and *TADA2B* (in module 8) (**Figure 3D**). Both genes were already validated for their pro-pluripotency roles (**Figure 1E,F, Supplemental Figure 4B,D**), so we set out to confirm their opposing roles in self-renewal. We used CRISPR-Cas9 targeting to generate multiple clonal knockout (KO) lines of *TADA2B* and *OTUD5*, which were confirmed by sequencing and western (**Figure 4A-D**). Consistent with our

screening results, *TADA2B* KOs demonstrated a higher growth rate than WT in E8 and E6 conditions (**Figure 4E,F**), whereas *OTUD5* KOs displayed reduced growth compared to WT in E6 medium (**Figure 4H**). We noticed that *OTUD5* KO hESCs did not display a significant growth defect in the standard hESC E8 culture condition (**Figure 4G**). To reconcile this finding with the E8 screening results, we speculate that *OTUD5* KO hESCs have compromised cell fitness, but the phenotype could be masked under optimal culture conditions. Supporting this idea, we found that *OTUD5* KO hESCs showed reduced growth in the E8 condition when the cells were challenged by passage without the Rho-associated protein kinase (ROCK) inhibitor Y-276325 (**Figure 4I**), normally used for optimal survival of dissociated hESCs during passaging. We further speculate that hESCs were more vulnerable in a large-scale CRISPR screening setting not only because the culture condition may be less-than-ideal, but also because of cell competition. To test the latter idea, we used lentiviruses to barcode individual KO and WT lines and cultured the cells together for a period of four weeks while collecting cells weekly to assess the representation of barcoded lines in culture. Representation of *OTUD5* KOs were greatly reduced over time while the representation of WT cells increased (**Figure 4J**). The divergence in self-renewal phenotype between module 6 and module 8, confirmed by phenotypic analysis of archetypal gene knockouts, makes clear that pro-pluripotency genes may exert opposing effect on self-renewal. These findings underscore the complexity of the relationship between self-renewal and pluripotent identity. As such, it is not sufficient to use self-renewal in hESC growth conditions as a proxy for pluripotent identity.

OTUD5, identified in module 8 along with a large number of chromatin regulators, is located in the nucleus [54–57], suggesting a role in chromatin regulation. To investigate this further, we performed chromatin-immunoprecipitation mass spectrometry (ChIP-MS) to identify chromatin factors associated with OTUD5 during early NE and DE differentiation (day 1) using *OTUD5* KO cells as a negative control (**Figure 4K-L, Table S4**). We found that OTUD5 was

associated with multiple known regulators of pluripotency including pro-pluripotency and pro-self-renewal hits identified in our screens. Notably, this included hits identified in the same module as *OTUD5*: SOX2, EP300, and multiple BAF complex members, the common ATPase of which, SMARCA4, was identified in module 8. A large proportion of OTUD5 ChIP-MS hits were also found to be associated with OCT4, a master pluripotency regulator and member of module 8, according to OCT4 ChIP-MS results (**Figure 4K-M, Table S4**). The top OTUD5 ChIP-MS hits were particularly enriched for regulators of active transcription and chromatin organization (**Figure 4N**), reflecting positive regulators of pluripotent identity and self-renewal found in our screens. Our findings indicate a previously underappreciated role for open chromatin in the stability and maintenance of the pluripotent cell state, and suggest that this process involves OTUD5 and the regulation of ubiquitination. Although OTUD5 has not been previously linked to pluripotency, our findings are consistent with the observation that knockout of *Otud5* in mice is embryonic lethal [57,58], and that OTUD5 regulates open chromatin in neuronal development [57].

Discussion

While PSCs are defined by both the ability to unlimitedly self-renew and maintain pluripotent identity [59–63], hPSC characterization, especially large-scale screening efforts, have largely focused on self-renewal [14]. A fundamental question that remains unanswered is whether pluripotent identity is regulated by the same mechanisms as self-renewal. Further, while pluripotency in development is transient and quickly transitions into the three germ layers, much of the research on pluripotency has been performed under continuously self-renewing PSC maintenance conditions. Our NE and DE screens represent the first genome-scale CRISPR-Cas9 loss-of-function screens to interrogate the dissolution of human pluripotent identity in dynamic transition states reflective of human development. The identification of shared hits between these NE and DE pluripotency screens suggests the existence of common

mechanisms regulating the dissolution of pluripotency independent of external differentiation signals, and expands on the current model of pluripotency that is dependent on the balance between differentiation programs [64]. The prevalence of chromatin regulators in these screens suggests a model of pluripotency beyond regulation by the core pluripotency factors OCT4, NANOG, and SOX2, and emphasizes the significance of chromatin alterations during the dissolution of the pluripotent state. While multiple epigenetic regulators have been shown to play a role in the maintenance of pluripotency [65], our screens in the context of dynamic transition states have identified a large number of regulators of open chromatin, including top hits such as EP300, BAF complex members, SAGA histone acetyltransferase members, and the deubiquitinase OTUD5.

Decoupling acquisition and loss of cell state in dynamic systems is particularly challenging. RNAi screens of iPSC reprogramming in a stage-specific manner showed that acquisition of pluripotency and down-regulation of the somatic cell gene network are distinct events, and both must be completed for successful reprogramming [66,67]. The dynamic nature of our screens for pluripotent cell identity allowed us to investigate the reverse: whether pluripotency dissolution during NE and DE differentiation involves separate forces that either propel the transitions to new cell states or push the cells away from the pluripotent state. Comparison of our DE context pluripotency screen, using *OCT4* as a readout, with previous DE differentiation screens from our lab, using *SOX17* as a readout [17] suggested the pull of differentiation signaling is distinct from the push of pluripotency loss. While top hits from the DE differentiation screen were by and large TFs or developmental signaling pathway components, in our DE pluripotency screen, many of the top hits were chromatin modifiers and transcriptional regulators, genes involved in RNA processing, and ubiquitin modifiers. It is remarkable that we discovered different gene regulatory programs by screens conducted on cells cultured in similar differentiation conditions but utilizing different marker genes, *OCT4* for pluripotency and *SOX17* for DE. The incorporation of more comprehensive single-cells readouts such as scRNA-seq [68–71]

in future studies will likely provide additional insights into the push and pull of cell-state transitions. Our screens provide an unbiased data set which can inform gene selection for further investigation of the push and pull of cell-state transitions and improvements to simple gene regulatory network models of cell-state transitions [72]. Beyond development, understanding the forces regulating the simultaneous acquisition and loss of alternative cell states is vital to the study of metaplasia and cell transformation leading to tumorigenesis. This is particularly important given the differing susceptibility of different lineages to transformation, even in response to the same stimuli [73].

By comparing the results from the NE and DE pluripotency screens with those from the E8 and E6 self-renewal screens, we discovered genes that play distinct roles in self-renewal and identity. The *OTUD5* and *TADA2B* gene knockout studies support these findings, indicating that studying pluripotency through the lens of self-renewal alone is insufficient. To effectively unravel pluripotency regulation, it is necessary to compare screens that assess different aspects of pluripotency, allowing for the identification of various regulatory mechanisms. In our work, we clustered genes based on multiple screen results, enabling the identification of related genes that function in the same complex or regulate the same cellular programs within the same modules. One module was enriched for hits that were positive regulators of pluripotent identity and self-renewal, including the core transcriptional regulators of pluripotency: *OCT4, NANOG,* and *SOX2,* and other known regulators of pluripotency. While clustering of screen results has been used to predict genetic relationships from CRISPR essentiality screens in cancer cell lines [93], our results demonstrate that such predictive clustering is possible using a small but targeted number of datasets, and may be further enhanced with incorporation of additional screening data from relevant differentiation contexts. This screening strategy and results may also be applied to understanding more mature stem cells in the stem cell niche. For example, hematopoietic stem cells, while highly proliferative, lose regenerative capacity over time as a result of this proliferation [75]. The ability to decouple regenerative capacity, driven by cell identity,

385 versus proliferation, is vital for cell engineering and advancing regenerative medicine. As such, the gene sets identified in this study have broad applicability and can be used to identify genes of interest in other biological systems. In hPSCs, understanding the regulation of pluripotency is fundamental to downstream differentiation efforts and the study of human development. The resources generated by this study lay the groundwork for large-scale discovery efforts involving
390 hPSC systems. For example, the NIH MorPhiC consortium aims to characterize knockout phenotypes in diverse human cell types for phenotypic analysis, and these resources will be instrumental in achieving this objective.

Author Contributions

B.P.R. and D.H. conceptualized the study, designed the experiments, interpreted results. B.P.R. performed most of the experiments. Q.V.L. assisted with the screens. H.C. performed clustering and Reactome analysis. D.L. and D.Y. performed the cell competition assay. S.G., S.S., J.Y., and R.L. performed ChIP-MS. N.V. generated the OCT4-GFP donor plasmid. J.R.D. assisted with characterization of KO lines. M.A.B. performed MAGeCK analysis. B.P.R. and D.H. wrote the manuscript. All authors provided editorial advice. D.H. supervised the study.

Acknowledgements

We thank H. Pan, P. Shila, and J. Giacalone for assisting with additional experiments not included in the manuscript; E. Apostolou and L. Studer for insightful discussions; and the MSKCC Gene Editing and Screening Core and the MSKCC Flow Cytometry Core for technical assistance. This study was supported in part by grants to D.H. from NIH (U01HG012051, UM1HG012654) and New York State Stem Cell Science (NYSTEM, C32593GG), MSKCC Cancer Center Support Grant from NIH (P30CA008748), an NIH T32 Training Grant (T32GM008539 to B.P.R.), a Howard Hughes Medical Institute (HHMI) Medical Research Fellowship (to N.V.), a NYSTEM training grant from the MSKCC Center for Stem Cell Biology (CSCB) (DOH01-TRAIN3-2015-2016-00006 to D.Y.).

Declaration of Interests

The authors declare no competing interests.

Methods

Culture of hESCs

Two human hESC lines were used in this study, H1 (NIHhESC-10-0043) and HUES8 (NIHhESC-09-0021), both with an inducible Cas9 insertion[20,76]. These lines were maintained in chemically defined, serum-free Essential 8 (E8) medium conditions (Thermo Fisher Scientific, A1517001) on tissue culture- treated polystyrene plates coated with vitronectin (Thermo Fisher Scientific, A14700) at 37 °C with 5% CO2. For regular maintenance, hESCs were dissociated with 0.5 mM EDTA (KD Medical, RGE-3130) at a 1:10–1:20 split ratio every 3–5 days. 10 μM Rho-associated protein kinase (ROCK) inhibitor Y-27632 (Selleck Chemicals, S1049) was added into the culture medium when passaging or thawing cells unless otherwise noted. Cells were counted using Vi-CELL XR Cell Viability Analyzer (Beckman Coulter). Cells were routinely confirmed to be Mycoplasma-free by the MSKCC Antibody and Bioresource Core Facility and karyotypically normal by the MSKCC Molecular Cytogenetics Core. All experiments were approved by the Tri-SCI Embryonic Stem Cell Research Oversight Committee.

Generation of H1 OCT4$^{GFP/+}$iCas9 Reporter Line

Generation of OCT4-2A-copGFP donor plasmid: The *OCT4*-GFP reporter construct was constructed using modifications to a selection free knock-in strategy previously used in our lab [19]. The donor vector for this construct was pOCT4-2A-copGFP. To generate this vector, an NheI-2A-copGFP-AscI cassette was PCR amplified using the primers NhPTV-F and Asc_St_copGFP-R from the plasmid pCRIIAgPTV_ppGFP (An AgeI-PTV1-2A-ppGFP fragment was amplified by PCR using AgPTVppGFP-F and ppGFP-R, using pMAX-GFP plasmid (Lonza) as template. The AgeI-P2A-ppGFP insert was purified and Topo-cloned into pCR™II-TOPO™ (Thermo Fisher Scientific) resulting in pCRIIAgPTV_ppGFP). Next, the NheI-2A-copGFP-AscI was ligated into the pCR™II-TOPO™ cloning vector using the TOPO TA Cloning Kit (Thermo Fisher Scientific, 450641) following manufacturers instructions for ligation

and transformation. Next, the pCR™II-TOPO™-NheI-2A- copGFP-AscI plasmid and the pOCT4-2A-copGFP plasmid were digested with NheI and AscI and ligated. Sequences for primers used for PCR and sequencing are listed in the **Table S5**.

Transfection into H1iCas9: Guide RNA (gRNA) and tracrRNA were ordered from IDT (Alt-R® CRISPR-Cas9 crRNA and #1072532). RNA molecules and plasmid were transiently transfected into hESCs using Lipofectamine 3000 (Thermo Fisher Scientific , L3000001) following manufacturer's instructions. Briefly, gRNA and tracrRNA were added at a 10 nM final concentration, 5µg donor plasmid was added. gRNA/tracrRNA and Lipofectamine/plasmid were diluted separately in Opti-MEM (Thermo Fisher Scientific , 31985070), mixed together, incubated for 15 min at room temperature (RT), and added dropwise to 500,000 freshly seeded iCas9 hESCs in one well of a 24-well plate. Cas9 expression was induced with 2 µg/ml doxycycline one day prior to transfection, the day of transfection, and one day after transfection. GFP positive clones were isolated through FACS and subsequent single cell colony picking. The H1 OCT4$^{GFP/+}$iCas9 reporter line is a heterozygous line as confirmed through PCR and DNA sequencing. *OCT4*-GFP reporter fidelity was confirmed by flow-cytometry analysis. gRNA sequences are listed in **Table S6**.

Flow Cytometry

Flow cytometry analysis were performed as previously described [17]. Antibodies used for flow cytometry are listed in **Key Resources Table**. Briefly, cells were dissociated and stained with DAPI for live GFP data collection or fixed and stained with LIVE-DEAD Fixable Violet Dead Cell Stain (Invitrogen; L34955) and corresponding antibodies for data collection using BD LSRFortessa or BD LSRII. Flow cytometry analysis and figures were generated in FlowJo v10. Gating strategy is shown in **Supplemental Figure 1D**.

Neuroectoderm Differentiation

Neuroectoderm differentiation performed as previously described [77] with modifications. hESC cultures were disaggregated using TrypLE (Life Technologies, 12563-029) for 4 minutes, collected in E8 media, spun at 200 x g for 5 minutes, and resuspended in E8 media. 400,000 cells per well of 6-well plate were seeded on vitronectin (Thermo Fisher Scientific, A14700) with 10 μM Rho-associated protein kinase (ROCK) inhibitor Y-27632 (Selleck Chemicals, S1049) in E8 medium (Thermo Fisher Scientific, A1517001). 24 hours after plating, cells were washed with PBS and exposed to Essential 6 (Thermo Fisher Scientific, A1516401) with 10μM SB431542 (Tocris, 161410) and 500nm LDN193189 (Cedarlane Labs, 04-0074-02). Media changed every 24hrs.

Definitive Endoderm Differentiation

Definitive Endoderm differentiation performed as previously described [78] with modifications. hESC cultures were disaggregated using TrypLE (Life Technologies, 12563-029) for 4 minutes, collected in E8 media, spun at 200 x g for 5 minutes, and resuspended in E8 media. 300,000 cells per well of 6-well plate were seeded on vitronectin (Thermo Fisher Scientific, A14700) with 10 μM Rho-associated protein kinase (ROCK) inhibitor Y-27632 (Selleck Chemicals, S1049) in E8 medium (Thermo Fisher Scientific, A1517001). 24 hours after plating, cells were washed with PBS and exposed to S1/S2 medium supplemented with 20 ng/ml Activin A (Bon-Opus Biosciences; C687-1mg) for 3 days, and CHIR99021 (Stemgent, 04-0004-10) for 2 days (first day, 5 μM; second day 0.5μM). S1/S2 medium was composed of MCDB131 medium (Thermo Fisher Scientific, 10372019) supplemented with 1.5g/L sodium bicarbonate (Research Products International, S22060), 1x Glutamax (Thermo Fisher Scientific, 35050061), 10mM glucose (Sigma-Aldrich, G8769), and 0.5% BSA (LAMPIRE, 7500804). Media changed every 24 hrs.

Infection and Expansion for Genome Wide CRISPR-Cas9 Screens

The human Brunello gRNA library [23], consisting of 76,441 guide RNAs (gRNAs) targeting 19,114 genes (four gRNAs per gene, was produced and tested as previously described [17]. A minimum of 200-fold library coverage is typically recommended for screens based on basic phenotypes such as cell survival and growth, given the relatively complex nature of our multiple reporter and essentiality screens, we target a 600X library coverage at all steps to maximize sensitivity. Around 140 million H1 OCT4$^{GFP/+}$iCas9 cells were harvested and infected with the lentiviral library at a low MOI of 0.4 at D0 in 150-mm plates at a density of 1.67 million per plate (85 plates total). 6 µg/ml protamine sulfate was added concurrently with the virus infection to enhance the infection efficiency. Infected cells were treated with 2 µg/ml doxycycline (Thermo Fisher Scientific, BP26535) (D1–D7) and 0.5 µg/ml puromycin (Sigma-Aldrich, P8833) (D2–D7). On D7, cells were treated with TrypLE Select (Thermo Fisher Scientific, 12563029), counted and replated for four individual screens.

Genome Wide CRISPR-Cas9 Screens for Pluripotency

For the NE screen, 160 million H1 OCT4$^{GFP/+}$ iCas9 cells were infected by the virus library, and then replated in 150-mm plates at a density of 8 million per plate (20 plates total). 24hrs after plating, on D8, cells were switched from maintenance E8 medium to NE differentiation medium (described in subsection *Neuroectoderm Differentiation*). After 36hrs of NE differentiation (D8-D9.5), cells were dissociated using TrypLE Select and sorted using FACSArias (BD Biosciences), according to GFP expression. Sorted GFP+ and GFP− cells were pelleted, and genomic DNA was immediately extracted using the QIAGEN Blood & Cell Culture DNA Maxi Kit (QIAGEN, 13362). For the DE screen, 90 million infected cells were replated in 150-mm plates at a plating density of 6 million per plate (15 plates total). 24hrs after plating, on D8, cells were switched from maintenance E8 medium to DE differentiation medium (described in subsection *Definitive Endoderm Differentiation*). After 60hrs of DE differentiation (D8-D10.5),

cells were dissociated using TrypLE Select and sorted using FACSArias (BD Biosciences), according to GFP expression. Sorted GFP+ and GFP− cells were pelleted, and genomic DNA was immediately extracted using the QIAGEN Blood & Cell Culture DNA Maxi Kit (QIAGEN, 13362). Hi-seq and data analysis was performed for each screen individually as previously described [17] to obtain gRNA readcounts.

Genome Wide CRISPR-Cas9 Screens for Self-Renewal

For the E8 and E6 screens, around 140 million H1 OCT4$^{GFP/+}$ iCas9 cells were infected by the virus library (library preparation and infection described in subsection *Infection and Expansion for Genome Wide CRISPR-Cas9 Screens*). Around 30 million cells were collected after antibiotic selection as Day 0 control. The remaining cells were split for the E8 and E6 screens. For the E8 screen, 66.5 million infected cells were replated in 150-mm plates at a density of 3.5 million cells per plate (19 plates total), these cells were allowed to expand and were split again at the same density with TrypLE Select on D11 and D14. Cells cultured in E8 were harvested with TrypLE Select and pelleted on D17. Genomic DNA was immediately extracted using the QIAGEN Blood & Cell Culture DNA Maxi Kit (QIAGEN, 13362). For the E6 screen, 66.5 million infected cells were replated in 150-mm plates at a density of 3.5 million cells per plate (19 plates total), 24hrs later (D8) medium was changed to Essential 6 (E6) medium conditions (Thermo Fisher Scientific, A1516401) and cultured in E6 medium for 120hrs, when medium was changed back to E8 (D13). 24hrs afterwards (D14) cells were split into 150-mm plates at a density of 3.5 million cells per plate (19 plates total) Cells cultured in E8 were harvested with TrypLE Select and pelleted on D17. Genomic DNA was immediately extracted using the QIAGEN Blood & Cell Culture DNA Maxi Kit (QIAGEN, 13362). Hi-seq and data analysis was performed for each screen individually as previously described[17] to obtain gRNA readcounts.

Pluripotency Screen Analysis

Genes were ranked by gRNA read count using the MAGeCK (model-based analysis of genome-wide CRISPR-Cas9 knockout) robust ranking aggregation (RRA) algorithm [24] using MAGeCK 0.5.9.4 default RRA parameters. In each screen, pro-pluripotency hits were defined as genes with 150 lowest ranked RRA scores (OCT4-GFP^{lo} enrichment), anti-per pluripotency hits were defined as genes with 150 lowest ranked RRA scores (OCT4-GFP^{hi} enrichment). Pluripotency scores calculated per screen per gene = log10(RRA score OCT4-GFP^{hi} enrichment) - log10(RRA score OCT4-GFP^{lo} enrichment). Log_2(Fold Change OCT4-GFP^{hi} / OCT4-GFP^{lo}) (LFC) also calculated. Screen results are found in **Table S1**. For GSEA top hit sets, genes were ranked by pluripotency score and GSEA performed with GSEA Software Version 4.2.3 [79,80] using pre-ranked option. Screening data plotted using ggplot2 R-package [81] formatted with Adobe Illustrator.

Comparison to Previous Differentiation Screens

For comparison to other screens, ectoderm differentiation screen data from Naxerova et al. [9] based on EpCAM+/NCAM- vs. EpCAM-/NCAM+ enrichment was used. These screens used 2 CRIPSR libraries covering roughly 2/3rs and 1/3rd of coding genome, published MaGECK analysis data for both ectoderm screen sets ("CRISPR Ectoderm P13 Mageck" and "CRISPR Ectoderm P2 Mageck") were combined, then all genes ranked by published RRA-scores. We defined pro-ectoderm differentiation hits as 150 genes with lowest neg. RRA score and anti-ectoderm differentiation hits as 150 genes with lowest pos. RRA score. Endoderm differentiation screen data from Li et al. [17] based on SOX17+ and SOX17- enrichment. We used "Brunello MaGECK" data set to define hits, pro- endoderm differentiation hits defined as 150 genes with the lowest pos. RRA score, and anti-endoderm differentiation hits defined as 150 genes with lowest neg. RRA score.

Comparison hit overlaps visualized with Upset plots [82] using the online implementation of UpsetR package [83] UpSetR Shiny App (https://gehlenborglab.shinyapps.io/upsetr/) which were then formatted with Adobe Illustrator. Analysis of hit lists performed with STRING database v11.5 [30] with enriched terms for "STRING clusters", "GO Component", and "COMPARTMENTS" shown. GO term enrichment analysis performed using Metascape 3.5 [31] (https://metascape.org/).

Self-Renewal Screen Analysis

Genes were ranked by gRNA read count using the MAGeCK (model-based analysis of genome-wide CRISPR-Cas9 knockout) robust ranking aggregation (RRA) algorithm [24] using MAGeCK 0.5.9.4 default RRA parameters. In each screen, pro-self-renewal hits were defined as genes with 150 lowest ranked RRA scores (Day 0 enrichment), anti-self-renewal hits were defined as genes with 150 lowest ranked RRA scores (Day 10 enrichment). Pluripotency scores calculated per screen per gene = log10(RRA score Day 10 enrichment) - log10(RRA score Day 0 enrichment). Log_2(Fold Change Day 0/ Day 10) (LFC) also calculated per gene. Screen results are found in **Table S1**.

Comparisons and Clustering Pluripotency and Self-Renewal Screens

Pearson correlation test UpSet plots, GSEA and STRING analysis performed as described in *Pluripotency Screen Analysis*. Enrichment analysis on the Reactome Pathway Database was performed on top 150 hits from each screen that could be uniquely identified by the Entrez ID using the Reactome-PA R package [41]. These Reactome sets were then ranked by Median |LFC| of the genes intersected with the top 150 gene group in the screen. For the hierarchical clustering of pro-pluripotency and pro-self-renewal screening hits, relative levels LFC were represented as column z-scores, and hierarchical clustering was done using the Pearson correlation chosen as the distance metric and Ward's algorithm as the linkage method.

The top 8 distinguished branches in the dendrogram were defined as modules. Modules were further characterized by STRING database V11.5 [30] using k-means clustering (k=5) with default parameters.

Comparisons to Self-Renewal and Essentiality Datasets

For comparison to other hESC self-renewal screens data from [11–13] was used, as re-analyzed in [12] by BAGEL analysis [84]. For all self-renewal screens, top 150 pro-self-renewal hits were calculated by highest Bayes Factor for fold change in late time point vs. early timepoint. Data for [12] screens were taken from the MEF "T12" set, and the Laminin "T12" set. [11] data was from the "day30" set, and [13] was from the "T18" data set. Common essentiality genes shown are the "CRISPRInferredCommonEssentials" data set from DepMap [43,44,46] version 22Q4 [42].

Pluripotency Screen Hit Validation

Hit validation was performed using the lentivirus CRISPR approach to generate knockouts in H1 OCT4$^{GFP/+}$iCas9 cells. gRNAs from the Brunello library are listed in **Table S6**. gRNAs were cloned into lentiGuide-puro (Addgene, 52963) following published protocols [85]. The lentiGuide-puro construct expresses a puromycin resistance gene, allowing for the selection of infected cells through puromycin treatment. 1 µg lentiGuide, 0.1 µg pCMV-VSV-G [86] (Addgene, 8454), and 0.4 µg psPAX2 (a gift from Didier Trono Addgene, 12260) plasmids were transfected with the JetPRIME reagent (VMR, 89137972) into 293T cells to pack lentiviruses. Viral supernatant was collected, aliquoted, and stored at −80 °C. A MOI of 0.30~0.36 was used for the infection of the H1 OCT4$^{GFP/+}$iCas9 cells with different lentiCRISPR viruses. 6 µg/ml protamine sulfate was added concurrently with the virus infection to enhance the infection efficiency. Reflecting screen conditions, infected cells were treated with 2 µg/ml doxycycline (D1–D7) and 0.5 µg/ml puromycin (D2–D7). On D7, cells were treated with TrypLE Select

(Thermo Fisher Scientific, 12563029), counted, and replated for validation. All replicates were performed starting from virus infection.

NE validation For NE validation D7 cells were replated in 6 well plates at 400,000 cells/well. 24hrs after plating, on D8, cells were switched from maintenance E8 medium to NE differentiation medium (described in the NE differentiation subsection). After 36hrs of NE differentiation (D8-D9.5), cells were dissociated using TrypLE Select and GFP levels were analyzed by flow cytometry. Relative intensity of OCT4-GFP = (Mean Fluorescent Intensity (M.F.I.) per gRNA) / (Experimental Mean (M.F.I. non-targeting controls)). All experimental repeats were performed starting from virus infection.

DE validation Given our observation that DE differentiation efficiency is density dependent, we were concerned that varying growth rates of knockout hESCs might affect DE differentiation and therefore the downregulation of pluripotency, even for genes that were not direct regulators of the dissolution of pluripotency in DE context. DE validation was performed with normalization to an in-well uninfected tdTomato (tdT)+ control, given the sensitivity of DE differentiation to variability in plating density. To generate the tdT+ control, H1 OCT4$^{GFP/+}$iCas9 cells were previously infected with virus containing the tdT containing plasmid pWPXL_Luc2tdT [87] which was a gift from Wenjun Guo. tdT+ clones were isolated through FACS and subsequent single cell colony picking. For DE validation D7 cells were co-plated with tdT+ cells at 150,000 cells/well of each for 300,000 cells/well total. 24hrs after plating, on D8, cells were switched from maintenance E8 medium to DE differentiation medium (described in the DE differentiation subsection). After 60hrs of DE differentiation (D8-D10.5), cells were dissociated using TrypLE Select and GFP levels were analyzed by flow cytometry. Relative intensity of OCT4-GFP = (M.F.I. per gRNA/M.F.I. in-well tdT+ control) / (Experimental Mean (M.F.I. non-targeting controls/M.F.I. in-well tdT+ controls for non-targeting gRNAs)). All experimental repeats were performed starting from virus infection.

Generation of Clonal Knockout hESCs

Clonal knockouts (KOs) were generated in the HUES8 iCas9 hESC [76] as previously described with some modifications [88]. Sequences for primers used for PCR and sequencing are listed in **Table S5**, and gRNA target sequences are listed in **Table S6**. Guide RNAs (gRNAs) and tracrRNA were ordered from IDT (Alt-R® CRISPR-Cas9 crRNA and #1072532). RNA molecules were transiently transfected into hESCs using Lipofectamine RNAiMAX (Thermo, 13778100) following manufacturer's instructions. Briefly, gRNA and tracrRNA were added at a 15 nM final concentration. gRNA/tracrRNA and Lipofectamine RNAiMAX were diluted separately in Opti-MEM (Thermo, 31985070), mixed together, incubated for 15 min at room temperature (RT), and added dropwise to 250,000 freshly seeded iCas9 hESCs in a 24-well plate. Cas9 expression was induced with 2 µg/ml doxycycline one day prior to transfection, the day of transfection, and one day after transfection. Three to four days after transfection, hESCs were dissociated to single cells using TrypLE Select (Thermo Fisher Scientific, 12563029), and 500-1000 cells were plated into one 100-mm tissue culture dish with 10 ml E8 media supplemented with 10 µM ROCK inhibitor Y-27632 (Selleck Chemicals, S1049) for colony formation. After 10 days of expansion, 96 colonies were picked into individual wells of a 96-well plate. gDNA from crude cell lysate was used for PCR genotyping, followed by expansion of KO cell lines. Additional sequencing performed on gDNA extracted by QIAGEN Blood & Cell Culture DNA Maxi Kit (QIAGEN, 13362), followed by PCR and insertion into Zero Blunt TOPO PCR Cloning Plasmid (Thermo Fisher Scientific , 450245) which were transfected and expanded per manufacturer instructions. Plasmid was miniprepped using the Zyppy Plasmid Miniprep Kit (Zymo, D4037) per manufacturer's instructions and sequenced. Clonal KOs were also confirmed by western blot.

Western Blots

Cell pellets were snap frozen in liquid nitrogen and lysed in cell lysis buffer (9803, Cell Signaling Technology) with proteinase/phosphatase inhibitors (5872, Cell Signaling Technology) and 1 mM PMSF (ICN19538105, MP Biomedicals). Proteins were precleared by centrifugation at 14,000g for 10 min at 4 °C. Protein concentration was determined by the Bradford Protein Assay (Bio-Rad, 500-0202). Equal amounts of protein were loaded into Bis-Tris 10% gel (Novex, NP0301BOX) and transferred to nitrocellulose membranes (Novex, LC2001). Membranes were blocked with 5% milk (LabScientific, M-0841). Primary antibody was incubated overnight at 4 °C. Membranes were washed with TBST three times for 10 min each and incubated with fluorescent conjugated secondary antibody for 1 h at room temperature. Membranes were washed with TBST three times for 10 min each. Blots were visualized using the Odyssey DLx Imaging System (LICOR) Antibodies used for western are listed in the **Key Resources Table.**

Growth Curves

hESCs were disaggregated using TrypLE Select and then mechanically dissociated into single cells using 1000 µl tips. One hundred thousand cells were plated into one well of a 6-well plate on vitronectin in E8 medium with ROCK inhibitor. Cells were subsequently maintained in E8 and harvested after TrypLE treatment every 24 hrs for counting cell numbers. For E6 growth curves, cells were rinsed with PBS and changed to Essential 6 (Thermo Fisher Scientific, A1516401) 24hrs after plating. For -ROCKi growth curves cells were plated in E8 without ROCK inhibitor.

Cell Competition Assay

Individual LARRY barcode constructs were cloned from the LARRY barcode library (Addgene:140024) [89] and transfected to 293T cells to generate lentivirus. Next, each OTUD5

KO and WT clone was infected with a unique LARRY barcode at low MOI. One week after lentiviral infection, the barcoded OTUD5 KO and WT cells, which expressed GFP, were sorted out. To do the cell competition test, an equal number of OTUD5 KO and WT cells were pooled and seeded in 6-well plates 200k per well. Cells were passaged every 3-4 days by TrypLE dissociation and 200k cells were seeded every time. 1, 2, 3 and 4 weeks after pooling, cells were collected for genomic DNA extraction. The LARRY barcodes were amplified via PCR. Primer sequences listed in **Table S5**. (The P5 and P7 adapters were then added to the LARRY PCR products to generate libraries and sequenced for 1 million reads per library. We used CRISPResso2 (http://crispresso.pinellolab.org/submission) [90] to quantify the representation of each barcode and thereby each cell line.

ChIP-MS and Analysis

OTUD5 ChIP-MS was performed on NE and DE Day 1 cells (differentiation described in the NE and DE differentiation subsections). OCT4 ChIP-MS was performed using hESCs grown in E8 conditions. ChIP-MS was performed from 15 million cells/experiment as previously described [21,91]. Antibodies used for immunoprecipitation are listed in the **Key Resources Table**. Proteins were eluted from the ChIP immunoprecipitation using a buffer containing 5% SDS (Thermo Fisher Scientific, AM9820) , 5 mM DTT (Thermo Fisher Scientific, FERR0861) and 50 mM ammonium bicarbonate (pH = 8), and left on the bench for about 1 hour for disulfide bond reduction. Samples were then alkylated with 20 mM iodoacetamide (VWR, IC10035105) in the dark for 30 minutes. Afterward, phosphoric acid (Thermo Fisher Scientific, A2421) was added to the sample at a final concentration of 1.2%. Samples were diluted in six volumes of binding buffer (90% methanol and 10 mM ammonium bicarbonate, pH 8.0). After gentle mixing, the protein solution was loaded to an S-trap filter (Protifi, C02-micro-80) and spun at 500 g for 30 sec. The sample was washed twice with binding buffer. Finally, 1 µg of sequencing grade trypsin (Promega, V5111), diluted in 50 mM ammonium bicarbonate, was added into the S-trap

filter and samples were digested at 37°C for 18 h. Peptides were eluted in three steps: (i) 40 µl of 50 mM ammonium bicarbonate, (ii) 40 µl of 0.1% TFA and (iii) 40 µl of 60% acetonitrile and 0.1% TFA. The peptide solution was pooled, spun at 1,000 g for 30 sec and dried in a vacuum centrifuge. Prior to mass spectrometry analysis, samples were desalted using a 96-well plate filter (Orochem) packed with 1 mg of Oasis HLB C-18 resin (Waters). Briefly, the samples were resuspended in 100 µl of 0.1% TFA and loaded onto the HLB resin, which was previously equilibrated using 100 µl of the same buffer. After washing with 100 µl of 0.1% TFA, the samples were eluted with a buffer containing 70 µl of 60% acetonitrile and 0.1% TFA and then dried in a vacuum centrifuge.

Samples were then resuspended in 10 µl of 0.1% TFA and loaded onto a Dionex RSLC Ultimate 300 (Thermo Scientific), coupled online with an Orbitrap Fusion Lumos (Thermo Scientific). Chromatographic separation was performed with a two-column system, consisting of a C-18 trap cartridge (300 µm ID, 5 mm length) and a picofrit analytical column (75 µm ID, 25 cm length) packed in-house with reversed-phase Repro-Sil Pur C18-AQ 3 µm resin. To analyze the proteome, peptides were separated using a 90 min gradient from 4-30% buffer B (buffer A: 0.1% formic acid, buffer B: 80% acetonitrile + 0.1% formic acid) at a flow rate of 300 nl/min. The mass spectrometer was set to acquire spectra in a data-dependent acquisition (DDA) mode. Briefly, the full MS scan was set to 300-1200 m/z in the orbitrap with a resolution of 120,000 (at 200 m/z) and an AGC target of 5x10e5. MS/MS was performed in the ion trap using the top speed mode (2 secs), an AGC target of 1x10e4 and an HCD collision energy of 35. Proteome raw files were searched using Proteome Discoverer software (v2.4, Thermo Scientific) using SEQUEST search engine and the SwissProt human database (updated June 2021). Each analysis was performed with three biological replicates. The search for total proteome included variable modification of N-terminal acetylation, and fixed modification of carbamidomethyl cysteine. Trypsin was specified as the digestive enzyme with up to 2 missed cleavages allowed. Mass tolerance was set to 10 pm for precursor ions and 0.2 Da for product ions. Peptide and protein false discovery rate was set to 1%. Following the search, data was processed as

previously described [92]. Briefly, proteins were log2 transformed, normalized by the average value of each sample and missing values were imputed using a normal distribution 2 standard deviations lower than the mean. Statistical regulation was assessed using heteroscedastic T-test (if p-value < 0.05). Data distribution was assumed to be normal but this was not formally tested. Interaction score and GO analysis for select hits determined by STRING online database [30] with visualization of network by Cytoscape [94].

Main Figures

Figure 1

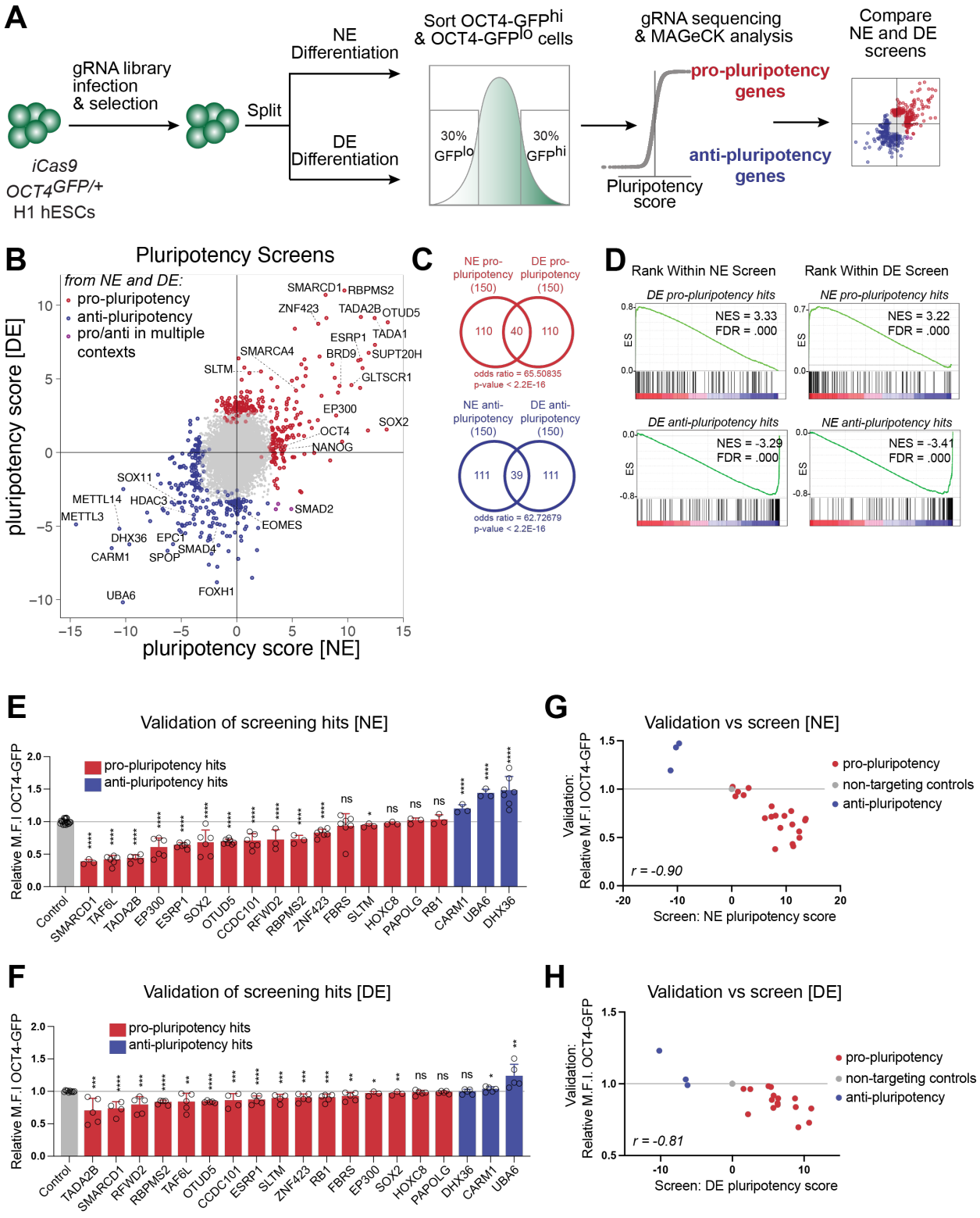

Figure 1. NE and DE screens for pluripotent identity reveal common program (A) Schematic of NE and DE CRISPR screen comparison. (B) NE and DE Screen results by pluripotency score per gene = log10(RRA score OCT4-GFP^{hi} enrichment) − log10(RRA score OCT4-GFP^{lo} enrichment), top 150 pro-pluripotency (ranked by RRA score OCT4-GFP^{lo} enrichment) and top 150 anti-pluripotency (ranked by RRA score OCT4-GFP^{hi} enrichment) hits from each screen labelled, RRA scores determined by MAGeCK. (C) Overlap of top 150 pro-pluripotency genes identified in NE vs. DE context screens, and top 150 anti-pluripotency genes identified in NE vs. DE context screens, Fisher's exact test (D) GSEA for enrichment of pro- and anti-pluripotency top hits in screen results ranked by pluripotency score, NE vs. DE screens. (E) Bar graphs show relative M.F.I. of OCT4-GFP following gRNA targeting in NE context. Relative M.F.I. OCT4-GFP = (Mean Fluorescent Intensity (M.F.I) per gRNA) / (M.F.I. non-targeting controls). *n*= 5 independent experiments. Data represented as mean. Error bars indicate s.d. P-values were obtained using one-way analysis of variance (ANOVA) followed by Dunnett multiple comparisons test. Significance is indicated as: * P<0.05, **P <0.01, ***P < 0.001, and **** P< 0.0001. (F) Bar graphs show relative M.F.I. of OCT4-GFP following gRNA targeting in DE context. Relative M.F.I. OCT4-GFP = (M.F.I. per gRNA/M.F.I. in-well tdT uninfected control) / (M.F.I. non-targeting controls/M.F.I. in-well tdT uninfected control). *n*= 5 independent experiments. (G) Comparison NE screen pluripotency score vs. NE validation relative intensity OCT4-GFP by gene. Statistical analysis by Pearson correlation test. (H) Comparison DE screen pluripotency score vs. DE validation relative intensity OCT4-GFP by gene.

Figure 2

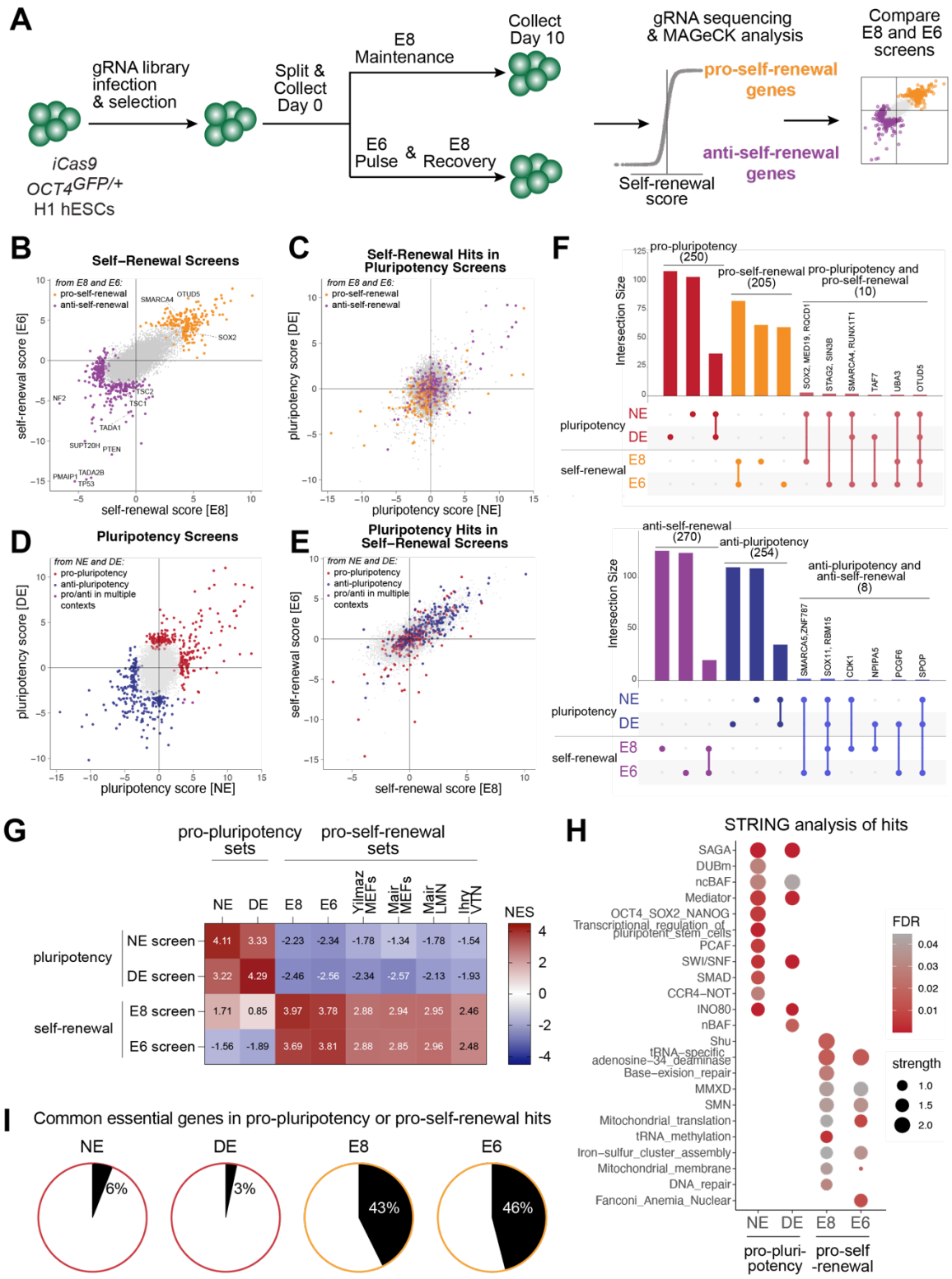
A
gRNA library infection & selection
Split & Collect Day 0
E8 Maintenance
Collect Day 10
E6 Pulse & E8 Recovery
iCas9
OCT4GFP/+
H1 hESCs
gRNA sequencing & MAGeCK analysis
pro-self-renewal genes
anti-self-renewal genes
Self-renewal score
Compare E8 and E6 screens
B
Self–Renewal Screens
from E8 and E6:
pro-self-renewal
anti-self-renewal
self-renewal score [E6]
self-renewal score [E8]
C
Self-Renewal Hits in Pluripotency Screens
pluripotency score [DE]
pluripotency score [NE]
D
Pluripotency Screens
from NE and DE:
pro-pluripotency
anti-pluripotency
pro/anti in multiple contexts
E
Pluripotency Hits in Self–Renewal Screens
F
pro-pluripotency (250)
pro-self-renewal (205)
pro-pluripotency and pro-self-renewal (10)
Intersection Size
pluripotency
self-renewal
NE
DE
E8
E6
anti-self-renewal (270)
anti-pluripotency (254)
anti-pluripotency and anti-self-renewal (8)
G
pro-pluripotency sets
pro-self-renewal sets
NE DE E8 E6 Yilmaz MEFs Mair MEFs Mair LMN Ihry VTN
NES
pluripotency
self-renewal
NE screen 4.11 3.33 -2.23 -2.34 -1.78 -1.34 -1.78 -1.54
DE screen 3.22 4.29 -2.46 -2.56 -2.34 -2.57 -2.13 -1.93
E8 screen 1.71 0.85 3.97 3.78 2.88 2.94 2.95 2.46
E6 screen -1.56 -1.89 3.69 3.81 2.88 2.85 2.96 2.48
H
STRING analysis of hits
SAGA
DUBm
ncBAF
Mediator
OCT4_SOX2_NANOG
Transcriptional_regulation_of_pluripotent_stem_cells
PCAF
SWI/SNF
SMAD
CCR4–NOT
INO80
nBAF
Shu
tRNA–specific adenosine–34–deaminase
Base–exision_repair
MMXD
SMN
Mitochondrial_translation
tRNA_methylation
Iron–sulfur_cluster_assembly
Mitochondrial_membrane
DNA_repair
Fanconi_Anemia_Nuclear
FDR
strength
pro-pluri-potency
pro-self -renewal
I
Common essential genes in pro-pluripotency or pro-self-renewal hits
NE 6%
DE 3%
E8 43%
E6 46%

Figure 2. Comparison pluripotency and self-renewal screens reveal distinct hits (A) Schematic E8 and E6 self-renewal screens. (B) E8 and E6 Screen results by self-renewal score per gene = log10(RRA score Day 10 enrichment) − log10(RRA score Day 0 enrichment), top 150 pro-self-renewal (ranked by RRA score Day 0 enrichment) and top 150 anti-self-renewal (ranked by RRA score Day 10 enrichment) hits from each screen labelled. (C) E8 and E6 screen self-renewal hits in NE and DE screens. (D) NE and DE Screen results by pluripotency score per gene = log10(RRA score OCT4-GFP^{hi} enrichment) − log10(RRA score OCT4-GFP^{lo} enrichment), top 150 pro-pluripotency (ranked by RRA score OCT4-GFP^{lo} enrichment) and top 150 anti-pluripotency (ranked by RRA score OCT4-GFP^{hi} enrichment). (E) NE and DE screen pluripotency hits in E8 and E6 screens. (F) Upset plot [82] of overlap NE, DE pro-pluripotency hits and E8, E6 pro-self-renewal, and upset plot overlap NE, DE anti-pluripotency and E8, E6 anti-self-renewal hits. (G) GSEA for enrichment of pro-pluripotency and pro-self-renewal gene sets from NE, DE, E8, E6 screens and previous screens by Yilmaz et al. [11], Mair et al. [12], and Ihry et al. [13], as re-analyzed by Mair et al. Gene sets from previous screens are top 150 genes per screen as ranked by Bayes factor score, calculated by BAGEL analysis [84] . (H) STRING[30] database analysis pro-pluripotency and pro-self-renewal hits from NE, DE, E8, and E6 screens, strength = log10(observed/expected) for enrichment of gene types within a set. (I) Proportion of common essentiality genes as defined by DepMap data sets [44,46,93] identified as top pro-pluripotency or pro-self-renewal hits in NE, DE, E8, and E6 screens.

Figure 3

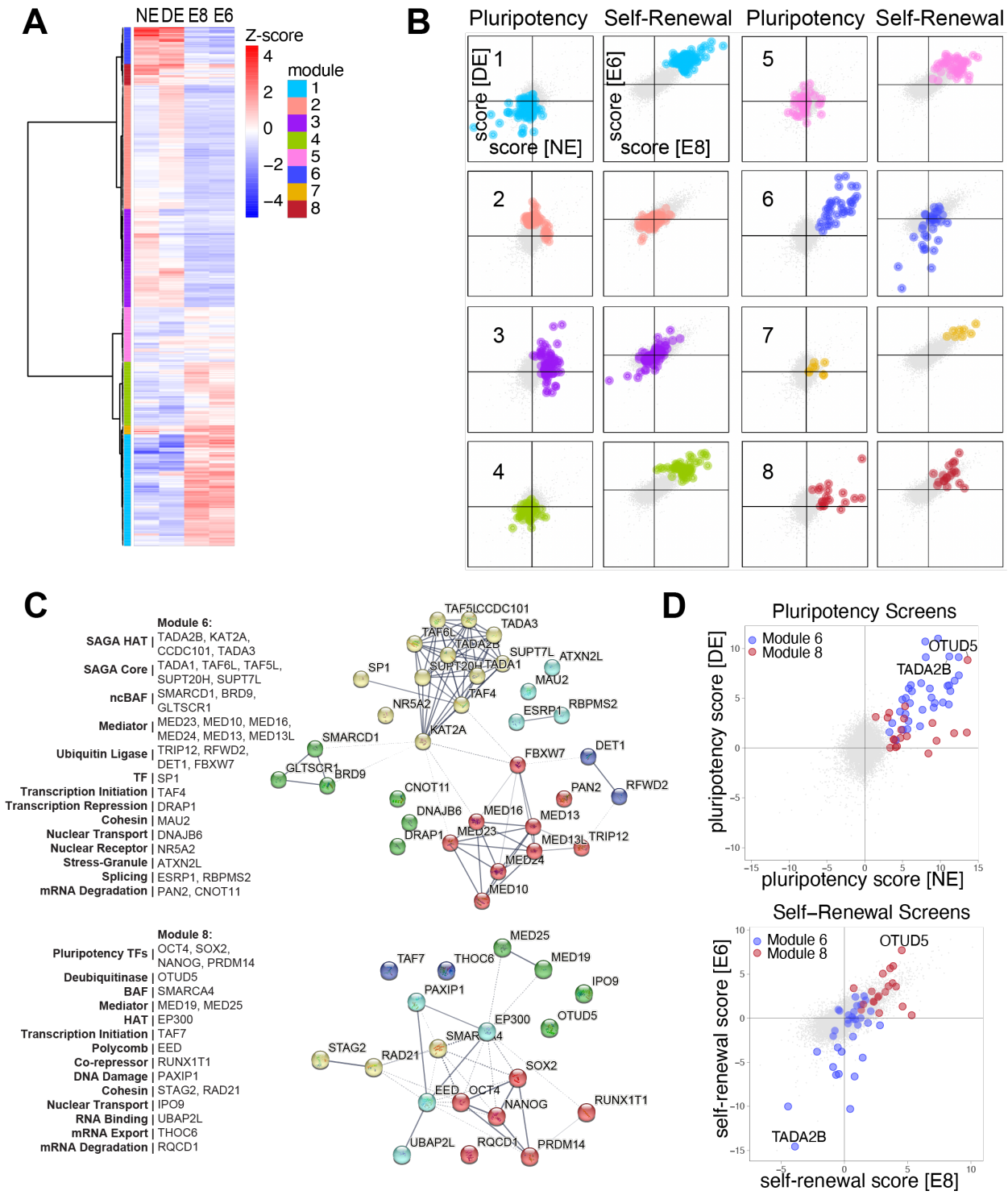
A
NE DE E8 E6
Z-score
4
2
0
−2
−4
module
1
2
3
4
5
6
7
8
B
Pluripotency
Self-Renewal
Pluripotency
Self-Renewal
score [DE]
score [NE]
score [E6]
score [E8]
C
Module 6:
SAGA HAT | TADA2B, KAT2A, CCDC101, TADA3
SAGA Core | TADA1, TAF6L, TAF5L, SUPT20H, SUPT7L
ncBAF | SMARCD1, BRD9, GLTSCR1
Mediator | MED23, MED10, MED16, MED24, MED13, MED13L
Ubiquitin Ligase | TRIP12, RFWD2, DET1, FBXW7
TF | SP1
Transcription Initiation | TAF4
Transcription Repression | DRAP1
Cohesin | MAU2
Nuclear Transport | DNAJB6
Nuclear Receptor | NR5A2
Stress-Granule | ATXN2L
Splicing | ESRP1, RBPMS2
mRNA Degradation | PAN2, CNOT11
Module 8:
Pluripotency TFs | OCT4, SOX2, NANOG, PRDM14
Deubiquitinase | OTUD5
BAF | SMARCA4
Mediator | MED19, MED25
HAT | EP300
Transcription Initiation | TAF7
Polycomb | EED
Co-repressor | RUNX1T1
DNA Damage | PAXIP1
Cohesin | STAG2, RAD21
Nuclear Transport | IPO9
RNA Binding | UBAP2L
mRNA Export | THOC6
mRNA Degradation | RQCD1
D
Pluripotency Screens
Module 6
Module 8
OTUD5
TADA2B
pluripotency score [DE]
pluripotency score [NE]
Self−Renewal Screens
Module 6
Module 8
OTUD5
TADA2B
self-renewal score [E6]
self-renewal score [E8]

Figure 3. Comparison of pluripotency and self-renewal hits reveal multiple gene modules

(A) Hierarchical clustering by z-score-per-gene of pro-pluripotency hits from NE and DE screens, and pro-self-renewal hits from E8 and E6 screens. Relative levels of LFC represented as column z-score. (B) Modules by pluripotency score in NE and DE screens, and self-renewal score in E8 and E6 screens. (C) Annotation of all genes within modules 6 and 8, and Interactome indicating known associations between members of module gene sets identified through STRING analysis using default parameters for high-confidence interactions. Each gene-set was further clustered using k-means clustering (k=5), and dotted lines indicate connections between clusters. (D) Modules 6 and 8 in NE and DE screens by pluripotency score, and E8 and E6 screens by self-renewal score with archetypal genes *TADA2B* and *OTUD5* labelled

Figure 4

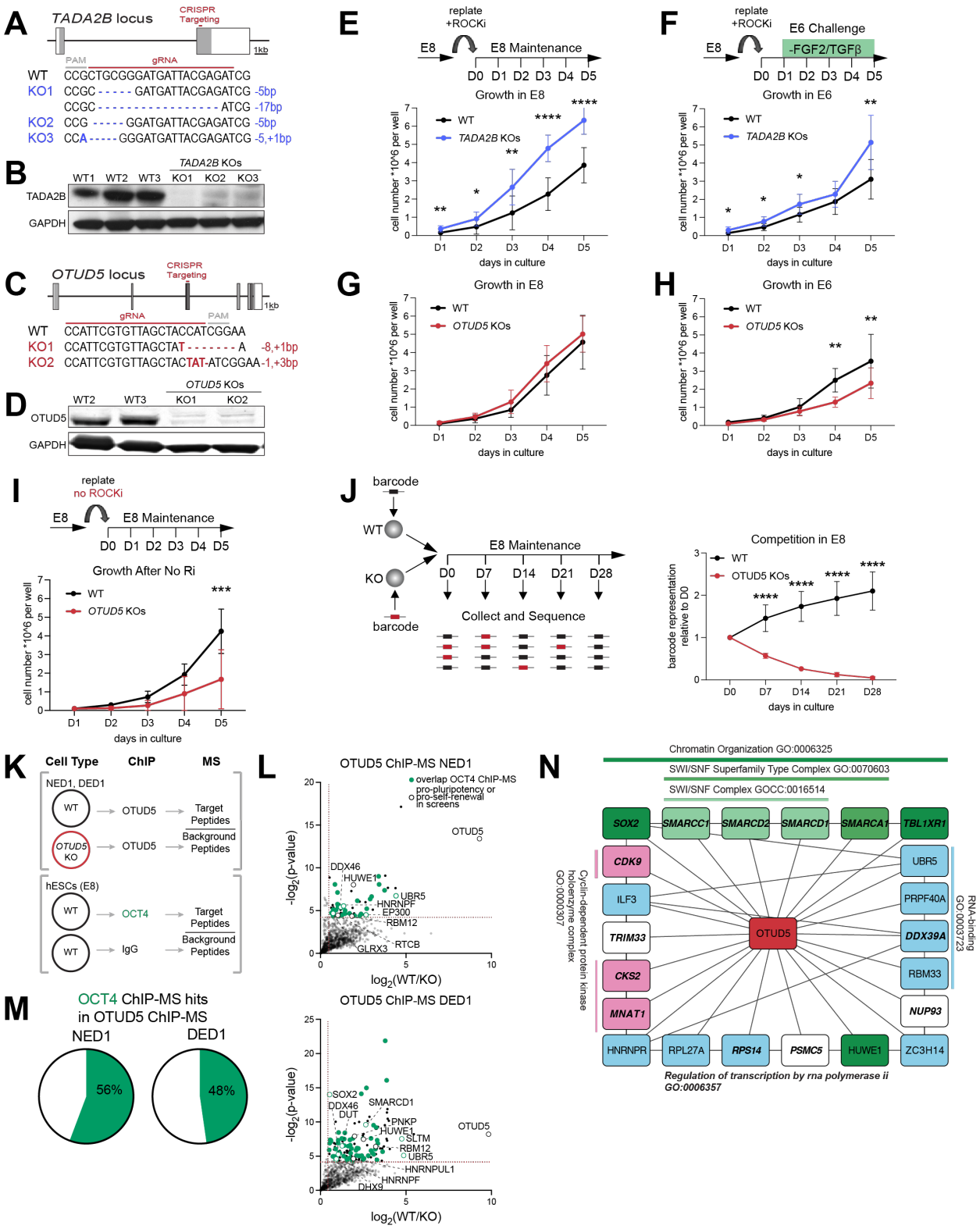
A
TADA2B locus
CRISPR Targeting
PAM
gRNA
1kb
WT CCGCTGCGGGATGATTACGAGATCG
KO1 CCGC - - - - - GATGATTACGAGATCG -5bp
CCGC - - - - - - - - - - - - - - - - - ATCG -17bp
KO2 CCG - - - - - GGATGATTACGAGATCG -5bp
KO3 CCA - - - - - GGGATGATTACGAGATCG -5,+1bp
B
TADA2B KOs
WT1 WT2 WT3 KO1 KO2 KO3
TADA2B
GAPDH
C
OTUD5 locus
CRISPR Targeting
gRNA
PAM
1kb
WT CCATTCGTGTTAGCTACCATCGGAA
KO1 CCATTCGTGTTAGCTAT - - - - - - - A -8,+1bp
KO2 CCATTCGTGTTAGCTACTAT-ATCGGAA -1,+3bp
D
OTUD5 KOs
WT2 WT3 KO1 KO2
OTUD5
GAPDH
E
replate +ROCKi
E8
E8 Maintenance
D0 D1 D2 D3 D4 D5
Growth in E8
WT
TADA2B KOs
cell number *10^6 per well
days in culture
F
replate +ROCKi
E6 Challenge
-FGF2/TGFβ
Growth in E6
G
Growth in E8
OTUD5 KOs
H
Growth in E6
I
replate no ROCKi
Growth After No Ri
J
barcode
WT
KO
E8 Maintenance
D0 D7 D14 D21 D28
Collect and Sequence
Competition in E8
OTUD5 KOs
barcode representation relative to D0
K
Cell Type
ChIP
MS
NED1, DED1
OTUD5 KO
Target Peptides
Background Peptides
hESCs (E8)
OCT4
IgG
L
OTUD5 ChIP-MS NED1
overlap OCT4 ChIP-MS
pro-pluripotency or pro-self-renewal in screens
OTUD5
DDX46
HUWE1
UBR5
HNRNPF
EP300
RBM12
RTCB
GLRX3
-log2(p-value)
log2(WT/KO)
OTUD5 ChIP-MS DED1
SOX2
SMARCD1
PNKP
SLTM
HNRNPUL1
DHX9
M
OCT4 ChIP-MS hits in OTUD5 ChIP-MS
NED1
DED1
56%
48%
N
Chromatin Organization GO:0006325
SWI/SNF Superfamily Type Complex GO:0070603
SWI/SNF Complex GOCC:0016514
SOX2
SMARCC1
SMARCD2
SMARCD1
SMARCA1
TBL1XR1
CDK9
ILF3
TRIM33
CKS2
MNAT1
OTUD5
UBR5
PRPF40A
DDX39A
RBM33
NUP93
HNRNPR
RPL27A
RPS14
PSMC5
HUWE1
ZC3H14
Cyclin-dependent protein kinase holoenzyme complex GO:0000307
RNA-binding GO:0003723
Regulation of transcription by rna polymerase ii GO:0006357

Figure 4. *TADA2B* KOs and *OTUD5* KOs have opposing self-renewal phenotype (A) Schematic of *TADA2B* including location of gRNA targeting and sequences of knockouts (KOs). Boxes indicate *TADA2B* exons, and filled grey boxes indicate the coding sequence of *TADA2B*. (B) Western blot of TADA2B confirming KOs. (C) Schematic of *OTUD5* targeting and KOs. (D) Western blot of OTUD5 confirming KOs. (E) Growth curve of WT and *TADA2B* KOs in E8 maintenance conditions and (F) E6 challenge conditions. 3 WT and 3 KO lines analyzed per experiment. *n*= 3 independent experiments. Data represented as mean. Error bars indicate s.d. Statistical analysis was performed by unpaired two-tailed Student's t-test. Significance is indicated as: * P<0.05, **P <0.01, ***P < 0.001, and **** P< 0.0001. (G) Growth curve of WT and *OTUD5* KOs in E8 maintenance conditions and (H) E6 challenge conditions. 2 WT and 2 KO lines analyzed per experiment. *n*= 3 independent experiments. (I) Growth curve of WT and *OTUD5* KOs after plating without Y-27632 (ROCKi), a standard component of hESC culture. (J) Cell competition assay WT vs. *OTUD5* KOs. Individual cell lines were labelled with LARRY barcodes [89], and pooled. Pooled cells were expanded in E8 conditions for 28 days. Pools were collected and sequenced for representation of barcodes every 7 days. (K) Schematic of OTUD5 and OCT4 ChIP-MS. (L) Plots showing proteins identified in OTUD5 ChIP-MS in NE Day 1 and DE Day 1. Dotted lines indicate the cut-offs (log2(Fold Change OCT4/IgG)) > 0.5, –log2 (P) > 4.32) for significantly enriched proteins. Proteins that are also identified by OCT4 ChIP-MS in hESCs are indicated with green circles. Pro-pluripotency and pro-self-renewal screen hits labelled. OTUD5 ChIP-MS *n* = 3 independent experiments. OCT4 ChIP-MS *n* = 2 independent experiments. (M) Proportion of proteins identified by OCT4 ChIP-MS in OTUD5 ChIP-MS hits. (N) Cytoscape network visualization displays the interactions between 22 hits identified by OTUD5 ChIP-MS. To select these hits, we merged the top 15 hits by p-value in NE and DE OTUD5 ChIP-MS, and only included those with interaction scores >0.4 with at least one other hits based on STRING analysis [30]. Edges and GO terms determined were determined by

STRING analysis. We also added edges visualizing the connection with OTUD5 from the ChIP-MS.

Supplemental Figures

Figure S1

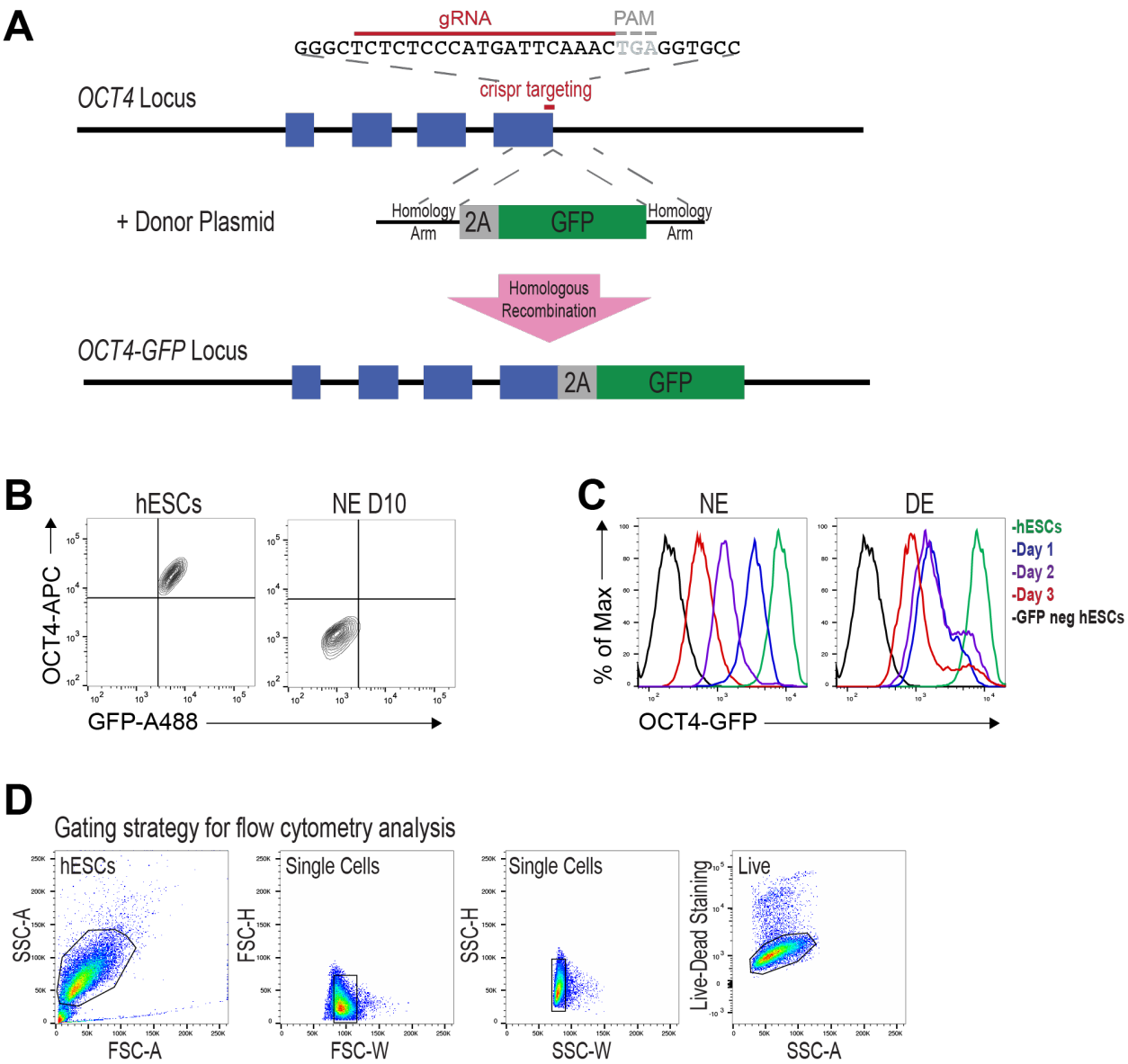

Figure S1 Generation of the *OCT4*-GFP reporter line (A) Knockin strategy for generating H1 OCT4$^{GFP/+}$ iCas9 hESCs. (B) Representative flow cytometry contour plots of OCT4$^{GFP/+}$ hESCs and OCT4$^{GFP/+}$ differentiated to day 10 of neuroectoderm (NE) differentiation co stained for OCT4 and GFP. Representative images are from 2 independent experiments. (C) Representative flow cytometry histograms of time-course of NE and definitive endoderm (DE) differentiations from OCT4$^{GFP/+}$ hESCs, OCT4$^{GFP/+}$ hESCs, and WT OCT4 $^{+/+}$ hESCs. Representative images are from 3 independent experiments (D) Flow cytometry gating strategy. The FSC-A/SSC-A gate identifies DE cells based on the size and granularity. The FSC-H/FSC-W and SSC-H/SSC-W gates identify single cells. Live-dead staining distinguishes live cells from dead cells.

Figure S2

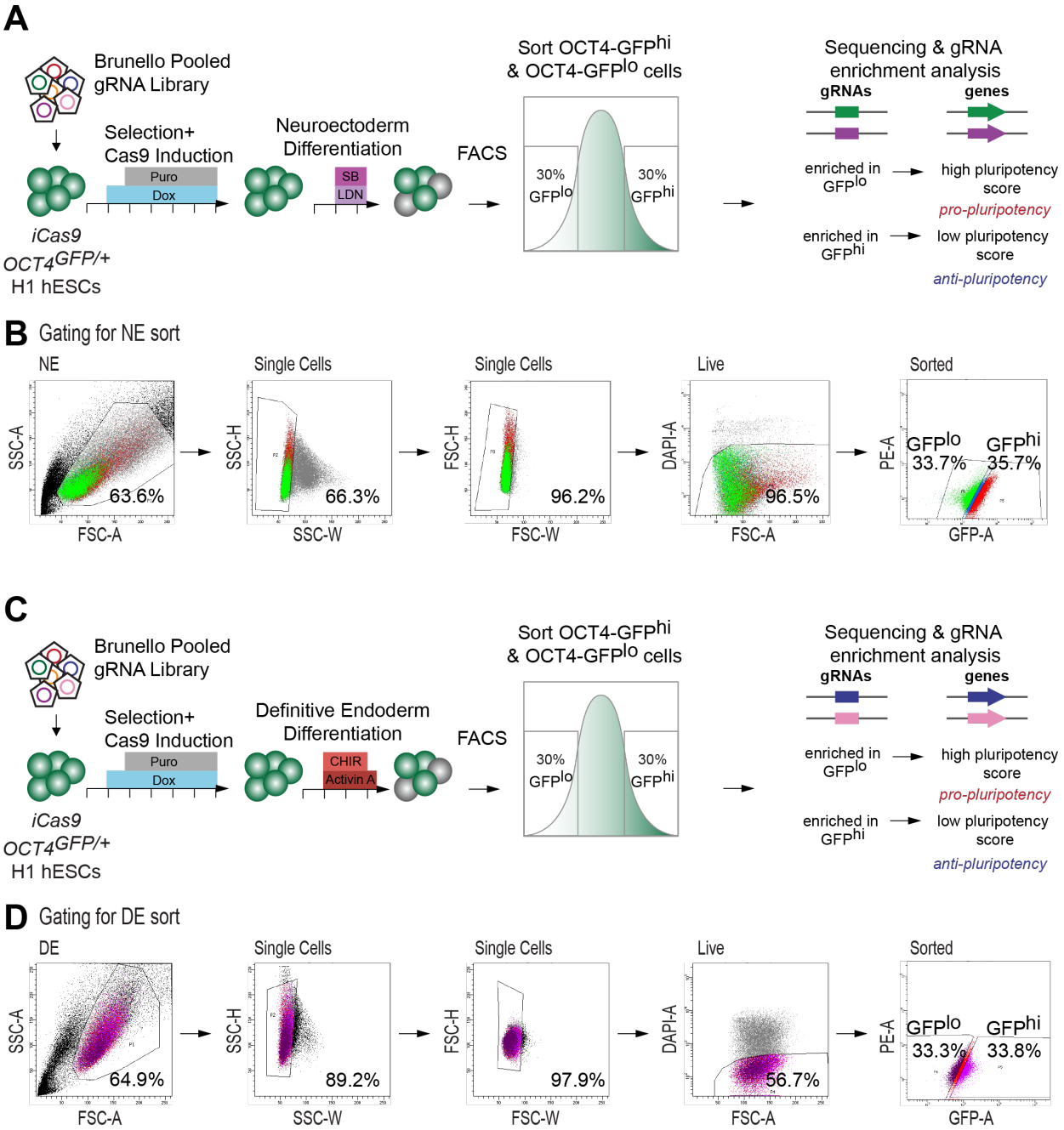
A
Brunello Pooled gRNA Library
Selection+ Cas9 Induction
Puro
Dox
iCas9
OCT4GFP/+
H1 hESCs
Neuroectoderm Differentiation
SB
LDN
FACS
Sort OCT4-GFPhi & OCT4-GFPlo cells
30% GFPlo
30% GFPhi
Sequencing & gRNA enrichment analysis
gRNAs
genes
enriched in GFPlo
high pluripotency score
pro-pluripotency
enriched in GFPhi
low pluripotency score
anti-pluripotency
B Gating for NE sort
NE
SSC-A
FSC-A
63.6%
Single Cells
SSC-H
SSC-W
66.3%
Single Cells
FSC-H
FSC-W
96.2%
Live
DAPI-A
FSC-A
96.5%
Sorted
PE-A
GFP-A
GFPlo 33.7%
GFPhi 35.7%
C
Brunello Pooled gRNA Library
Selection+ Cas9 Induction
Puro
Dox
iCas9
OCT4GFP/+
H1 hESCs
Definitive Endoderm Differentiation
CHIR
Activin A
FACS
Sort OCT4-GFPhi & OCT4-GFPlo cells
30% GFPlo
30% GFPhi
Sequencing & gRNA enrichment analysis
gRNAs
genes
enriched in GFPlo
high pluripotency score
pro-pluripotency
enriched in GFPhi
low pluripotency score
anti-pluripotency
D Gating for DE sort
DE
SSC-A
FSC-A
64.9%
Single Cells
SSC-H
SSC-W
89.2%
Single Cells
FSC-H
FSC-W
97.9%
Live
DAPI-A
FSC-A
56.7%
Sorted
PE-A
GFP-A
GFPlo 33.3%
GFPhi 33.8%

Figure S2. Genome-scale screens to identify regulators of the dissolution of pluripotency in neuroectoderm (NE) and definitive endoderm (DE) contexts (A) NE CRISPR screen schematic. Each line segment on the horizontal arrows indicates 1 d of media and chemical treatment. (B) Gating used for flow-sorting GFP^{hi} and GFP^{lo} in NE screen (C) DE CRISPR screen schematic and (D) gating.

Figure S3

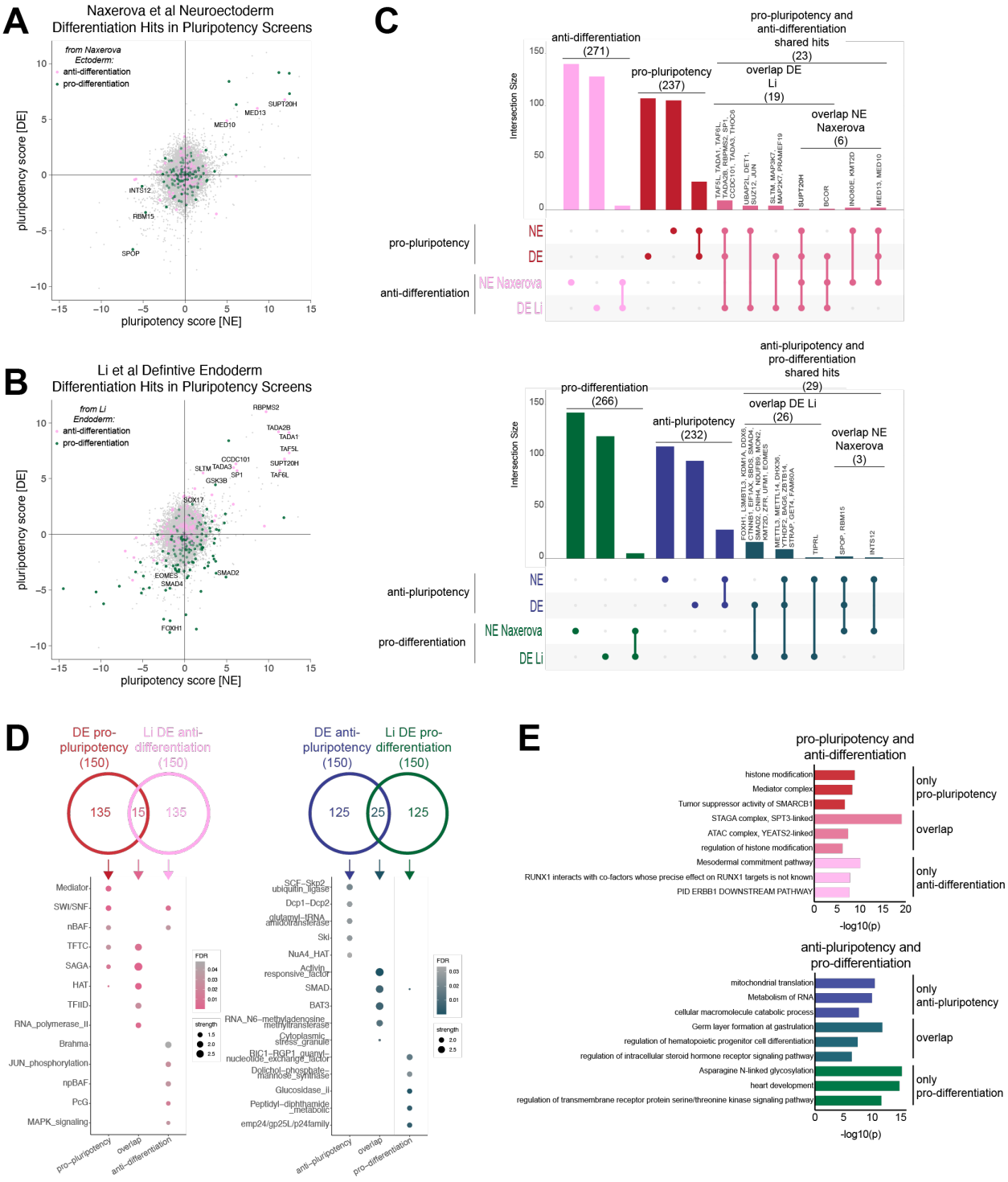
A
Naxerova et al Neuroectoderm Differentiation Hits in Pluripotency Screens
from Naxerova Ectoderm:
anti-differentiation
pro-differentiation
pluripotency score [DE]
pluripotency score [NE]
B
Li et al Defintive Endoderm Differentiation Hits in Pluripotency Screens
from Li Endoderm:
anti-differentiation
pro-differentiation
C
Intersection Size
anti-differentiation (271)
pro-pluripotency (237)
pro-pluripotency and anti-differentiation shared hits (23)
overlap DE Li (19)
overlap NE Naxerova (6)
pro-pluripotency
anti-differentiation
NE
DE
NE Naxerova
DE Li
pro-differentiation (266)
anti-pluripotency (232)
anti-pluripotency and pro-differentiation shared hits (29)
overlap DE Li (26)
overlap NE Naxerova (3)
anti-pluripotency
pro-differentiation
D
DE pro-pluripotency (150)
Li DE anti-differentiation (150)
135
15
135
DE anti-pluripotency (150)
Li DE pro-differentiation (150)
125
25
125
Mediator
SWI/SNF
nBAF
TFTC
SAGA
HAT
TFIID
RNA_polymerase_II
Brahma
JUN_phosphorylation
npBAF
PcG
MAPK_signaling
pro-pluripotency
overlap
anti-differentiation
SCF-Skp2 ubiquitin ligase
Dcp1-Dcp2
glutamyl-tRNA amidotransferase
Ski
NuA4_HAT
Activin responsive factor
SMAD
BAT3
RNA_N6-methyladenosine methyltransferase
Cytoplasmic stress granule
RIC1-RGP1 guanyl-nucleotide exchange factor
Dolichol-phosphate-mannose synthase
Glucosidase_II
Peptidyl-diphthamide metabolic
emp24/gp25L/p24family
anti-pluripotency
overlap
pro-differentiation
FDR
strength
E
pro-pluripotency and anti-differentiation
histone modification
Mediator complex
Tumor suppressor activity of SMARCB1
STAGA complex, SPT3-linked
ATAC complex, YEATS2-linked
regulation of histone modification
Mesodermal commitment pathway
RUNX1 interacts with co-factors whose precise effect on RUNX1 targets is not known
PID ERBB1 DOWNSTREAM PATHWAY
only pro-pluripotency
overlap
only anti-differentiation
-log10(p)
anti-pluripotency and pro-differentiation
mitochondrial translation
Metabolism of RNA
cellular macromolecule catabolic process
Germ layer formation at gastrulation
regulation of hematopoietic progenitor cell differentiation
regulation of intracellular steroid hormone receptor signaling pathway
Asparagine N-linked glycosylation
heart development
regulation of transmembrane receptor protein serine/threonine kinase signaling pathway
only anti-pluripotency
overlap
only pro-differentiation
-log10(p)

Figure S3. Pluripotency versus differentiation competence screens reveal distinct regulatory networks (A) Top 150 pro-ectoderm and top 150 anti-ectoderm hits from Naxerova et al.[9] (ranked by RRA scores for enrichment in EpCAM+/NCAM- and EpCAM-/NCAM+ populations respectively) in NE and DE screens for pluripotency. (B) Top 150 pro-endoderm and top 150 anti-endoderm hits from Li et al.[17] (ranked by RRA scores for enrichment in SOX17- and SOX17+ populations respectively) in NE and DE screens for pluripotency. (C) Overlap of NE and DE pro-pluripotency hits, anti-ectoderm hits, and anti-endoderm hits as shown by Upset plot, and overlap of NE and DE anti-pluripotency hits, Naxerova et al. pro-ectoderm hits, and Li et al. pro-endoderm hits. (D) STRING database analysis overlapping and non-overlapping hits from DE pluripotency screen and Li et al endoderm screen, strength = log10(observed/expected) for enrichment of gene types within a set. (E) GO term enrichment analysis as performed by Metascape [31] of overlapping and non-overlapping hits from DE pluripotency screen and endoderm screen.

Figure S4

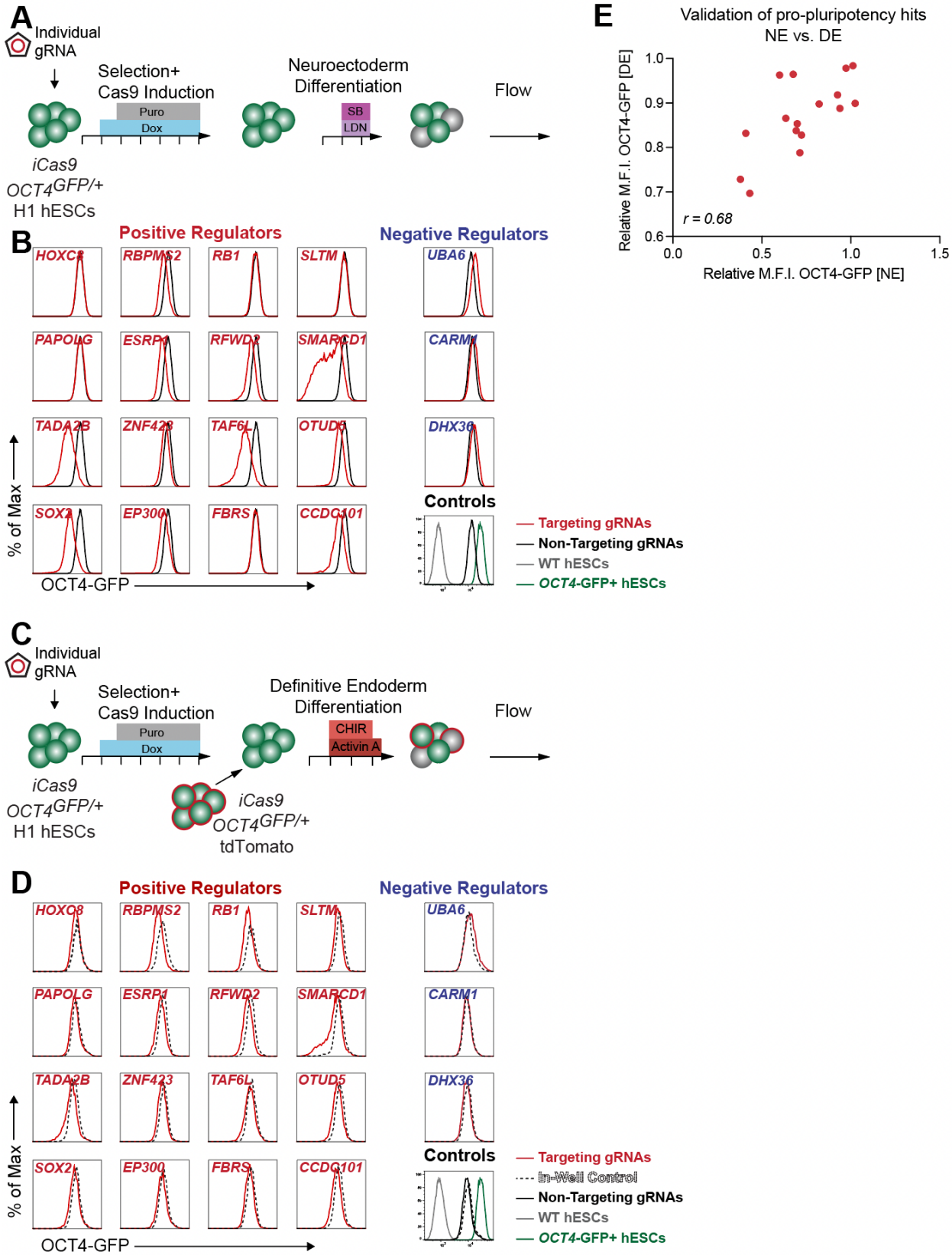
A
Individual gRNA
Selection+ Cas9 Induction
Puro
Dox
Neuroectoderm Differentiation
SB
LDN
Flow
iCas9 OCT4GFP/+ H1 hESCs
B
Positive Regulators
Negative Regulators
HOXC8
RBPMS2
RB1
SLTM
UBA6
PAPOLG
ESRP1
RFWD2
SMARCD1
CARM1
TADA2B
ZNF423
TAF6L
OTUD5
DHX36
SOX2
EP300
FBRS
CCDC101
Controls
% of Max
OCT4-GFP
Targeting gRNAs
Non-Targeting gRNAs
WT hESCs
OCT4-GFP+ hESCs
C
Individual gRNA
Selection+ Cas9 Induction
Puro
Dox
Definitive Endoderm Differentiation
CHIR
Activin A
Flow
iCas9 OCT4GFP/+ H1 hESCs
iCas9 OCT4GFP/+ tdTomato
D
Positive Regulators
Negative Regulators
HOXC8
RBPMS2
RB1
SLTM
UBA6
PAPOLG
ESRP1
RFWD2
SMARCD1
CARM1
TADA2B
ZNF423
TAF6L
OTUD5
DHX36
SOX2
EP300
FBRS
CCDC101
Controls
% of Max
OCT4-GFP
Targeting gRNAs
In-Well Control
Non-Targeting gRNAs
WT hESCs
OCT4-GFP+ hESCs
E
Validation of pro-pluripotency hits
NE vs. DE
Relative M.F.I. OCT4-GFP [DE]
Relative M.F.I. OCT4-GFP [NE]
r = 0.68
1.0
0.9
0.8
0.7
0.6
0.0
0.5
1.0
1.5

Figure S4. Validation of NE and DE pluripotency screen hits (A) Schematic of hit validation in NE context using lentiCRISPR infection. (B) Flow cytometry histograms show fluorescence OCT4-GFP following gRNA targeting in NE context. Representative images from one of five independent experiments. (C) Schematic of hit validation in DE context using lentiCRISPR infection, including in-well uninfected tdTomato (tdT) control. (D) Flow cytometry histograms show fluorescence OCT4-GFP following gRNA targeting in DE context. Representative images from one of five independent experiments. (E) Comparison NE context validation to DE context validation. Relative M.F.I. OCT4-GFP [NE] = (M.F.I. per gRNA) / (M.F.I. non-targeting controls). Relative M.F.I. OCT4-GFP [DE] = (M.F.I. per gRNA/M.F.I. in-well tdT uninfected control) / (M.F.I. non-targeting controls/M.F.I. in-well tdT uninfected control). Mean *n*=5.

Figure S5

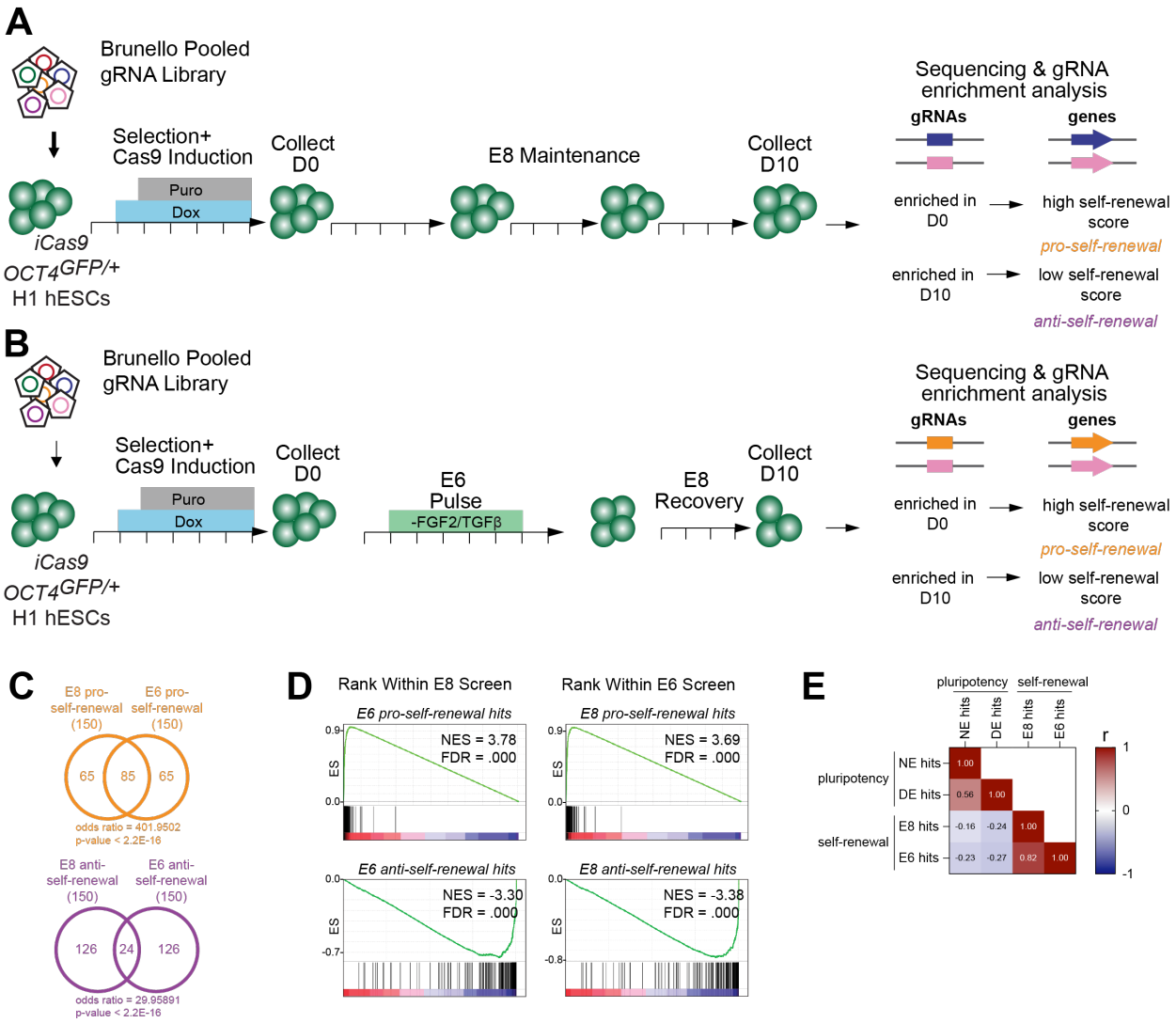
A
Brunello Pooled gRNA Library
Selection+ Cas9 Induction
Puro
Dox
Collect D0
E8 Maintenance
Collect D10
iCas9
OCT4GFP/+
H1 hESCs
Sequencing & gRNA enrichment analysis
gRNAs
genes
enriched in D0
high self-renewal score
pro-self-renewal
enriched in D10
low self-renewal score
anti-self-renewal
B
Brunello Pooled gRNA Library
Selection+ Cas9 Induction
Puro
Dox
Collect D0
E6 Pulse
-FGF2/TGFβ
E8 Recovery
Collect D10
iCas9
OCT4GFP/+
H1 hESCs
Sequencing & gRNA enrichment analysis
gRNAs
genes
enriched in D0
high self-renewal score
pro-self-renewal
enriched in D10
low self-renewal score
anti-self-renewal
C
E8 pro-self-renewal (150)
E6 pro-self-renewal (150)
65
85
65
odds ratio = 401.9502
p-value < 2.2E-16
E8 anti-self-renewal (150)
E6 anti-self-renewal (150)
126
24
126
odds ratio = 29.95891
p-value < 2.2E-16
D
Rank Within E8 Screen
Rank Within E6 Screen
E6 pro-self-renewal hits
NES = 3.78
FDR = .000
E8 pro-self-renewal hits
NES = 3.69
FDR = .000
E6 anti-self-renewal hits
NES = -3.30
FDR = .000
E8 anti-self-renewal hits
NES = -3.38
FDR = .000
ES
E
pluripotency
self-renewal
NE hits
DE hits
E8 hits
E6 hits
1.00
0.56
1.00
-0.16
-0.24
1.00
-0.23
-0.27
0.82
1.00
r
1
0
-1

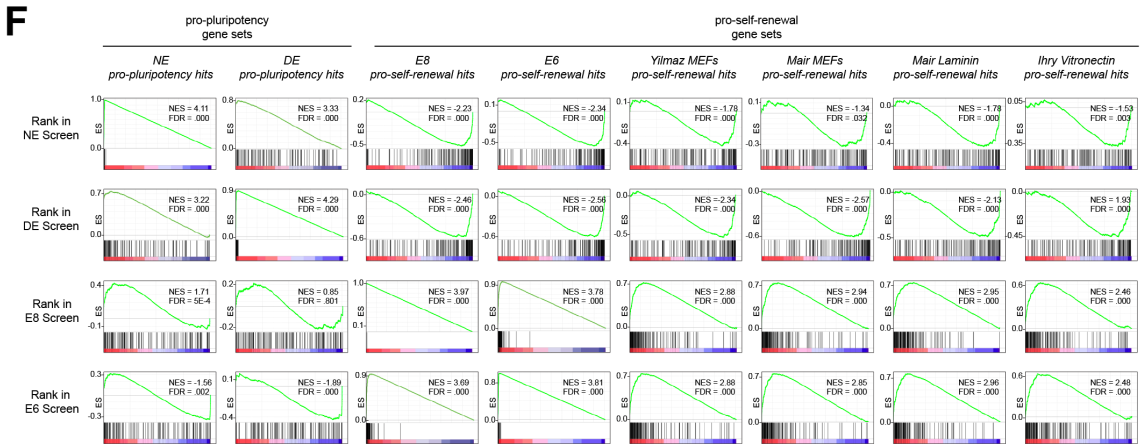
F
pro-pluripotency gene sets
pro-self-renewal gene sets
NE pro-pluripotency hits
DE pro-pluripotency hits
E8 pro-self-renewal hits
E6 pro-self-renewal hits
Yilmaz MEFs pro-self-renewal hits
Mair MEFs pro-self-renewal hits
Mair Laminin pro-self-renewal hits
Ihry Vitronectin pro-self-renewal hits
Rank in NE Screen
Rank in DE Screen
Rank in E8 Screen
Rank in E6 Screen
ES

Figure S5. E8 and E6 context self-renewal screens reveal common hits (A) E8 CRISPR screen schematic. Each line segment on the horizontal arrows indicates 1 d of media and chemical treatment. (B) E6 CRISPR screen schematic. (C) Overlap of top 150 pro-self-renewal genes identified in E8 vs. E6 context screens, and top 150 anti-self-renewal genes identified in E8 vs. E6 context screens, Fisher's exact test. (D) GSEA for enrichment of pro- and anti-self-renewal top hits in screen results ranked by self-renewal score, E8 vs. E6 screens. (E) Pearson correlation tests of hits by pluripotency or self-renewal score. (F) details of GSEA for enrichment of pro-pluripotency and pro-self renewal gene sets from NE, DE, E8, E6 screens and previous screens by Yilmaz et al., Mair et al., and Ihry et al. [11–13] in our NE, DE, E8, and E6 screens. Gene sets from previous screens are top 150 pro-self-renewal genes per screen as ranked by Bayes factor score, calculated by BAGEL analysis[84] as re-analyzed by Mair et al.

Figure S6

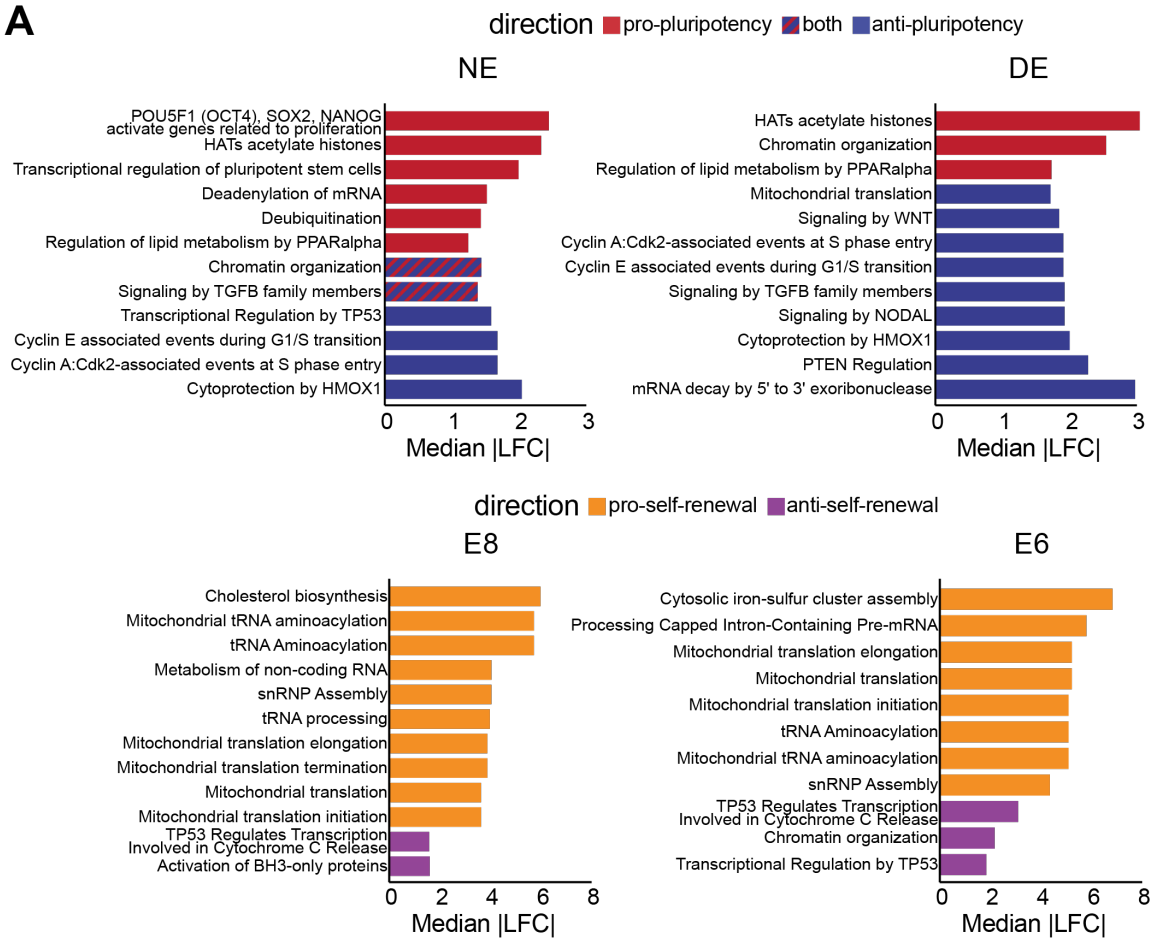
A
direction pro-pluripotency both anti-pluripotency
NE
POU5F1 (OCT4), SOX2, NANOG activate genes related to proliferation
HATs acetylate histones
Transcriptional regulation of pluripotent stem cells
Deadenylation of mRNA
Deubiquitination
Regulation of lipid metabolism by PPARalpha
Chromatin organization
Signaling by TGFB family members
Transcriptional Regulation by TP53
Cyclin E associated events during G1/S transition
Cyclin A:Cdk2-associated events at S phase entry
Cytoprotection by HMOX1
0 1 2 3
Median |LFC|
DE
HATs acetylate histones
Chromatin organization
Regulation of lipid metabolism by PPARalpha
Mitochondrial translation
Signaling by WNT
Cyclin A:Cdk2-associated events at S phase entry
Cyclin E associated events during G1/S transition
Signaling by TGFB family members
Signaling by NODAL
Cytoprotection by HMOX1
PTEN Regulation
mRNA decay by 5' to 3' exoribonuclease
0 1 2 3
Median |LFC|
direction pro-self-renewal anti-self-renewal
E8
Cholesterol biosynthesis
Mitochondrial tRNA aminoacylation
tRNA Aminoacylation
Metabolism of non-coding RNA
snRNP Assembly
tRNA processing
Mitochondrial translation elongation
Mitochondrial translation termination
Mitochondrial translation
Mitochondrial translation initiation
TP53 Regulates Transcription Involved in Cytochrome C Release
Activation of BH3-only proteins
0 2 4 6 8
Median |LFC|
E6
Cytosolic iron-sulfur cluster assembly
Processing Capped Intron-Containing Pre-mRNA
Mitochondrial translation elongation
Mitochondrial translation
Mitochondrial translation initiation
tRNA Aminoacylation
Mitochondrial tRNA aminoacylation
snRNP Assembly
TP53 Regulates Transcription Involved in Cytochrome C Release
Chromatin organization
Transcriptional Regulation by TP53
0 2 4 6 8
Median |LFC|

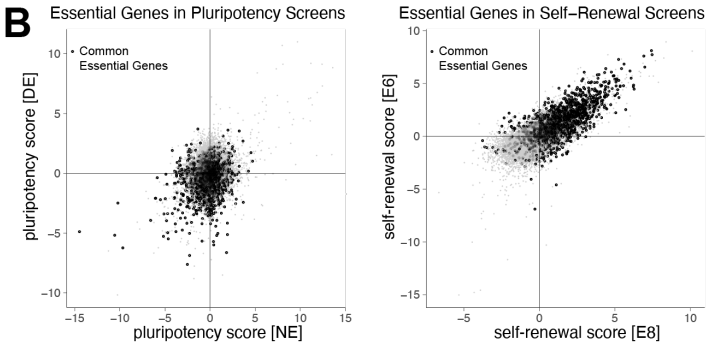
B
Essential Genes in Pluripotency Screens
Common Essential Genes
pluripotency score [DE]
pluripotency score [NE]
Essential Genes in Self−Renewal Screens
Common Essential Genes
self-renewal score [E6]
self-renewal score [E8]

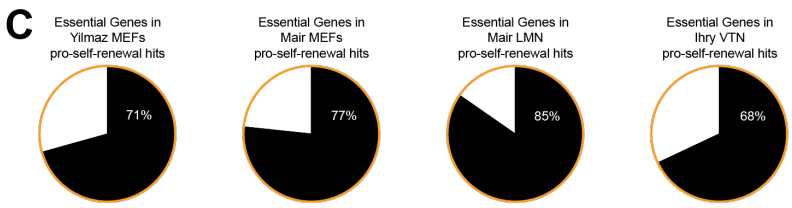
C
Essential Genes in Yilmaz MEFs pro-self-renewal hits
71%
Essential Genes in Mair MEFs pro-self-renewal hits
77%
Essential Genes in Mair LMN pro-self-renewal hits
85%
Essential Genes in Ihry VTN pro-self-renewal hits
68%

Figure S6. Distinct regulation of pluripotency and self-renewal (A) Top reactome pathway analysis gene sets which score in the pro direction, anti direction, or both. Gene sets identified in top hits of pro-pluripotency, anti-pluripotency, pro-self-renewal, and anti-self-renewal NE, DE, E8, and E6 screen hits. Median |Log_2(Fold Change of OCT4-GFP^{lo}/OCT4-GFP^{hi})| or |Log_2(Fold Change of Day 0/Day 10)| (LFC) from screen calculated for hits identified in reactome set. Highest absolute median |LFC| sets shown. For gene sets identified in both pro and anti directions, mean of median |LFC| calculated for both sets shown. (B) Common essentiality genes by pluripotency score in NE and DE screens, and self-renewal score in E8 and E6 screens. (C) Proportion of common essentiality genes identified in pro-self renewal gene sets from previous screens by Yilmaz et al., Mair et al., and Ihry et al., as re-analyzed by Mair et al. [11–13] Gene sets from previous screens are top 150 genes per screen as ranked by Bayes factor score, calculated by BAGEL analysis [84].

Figure S7

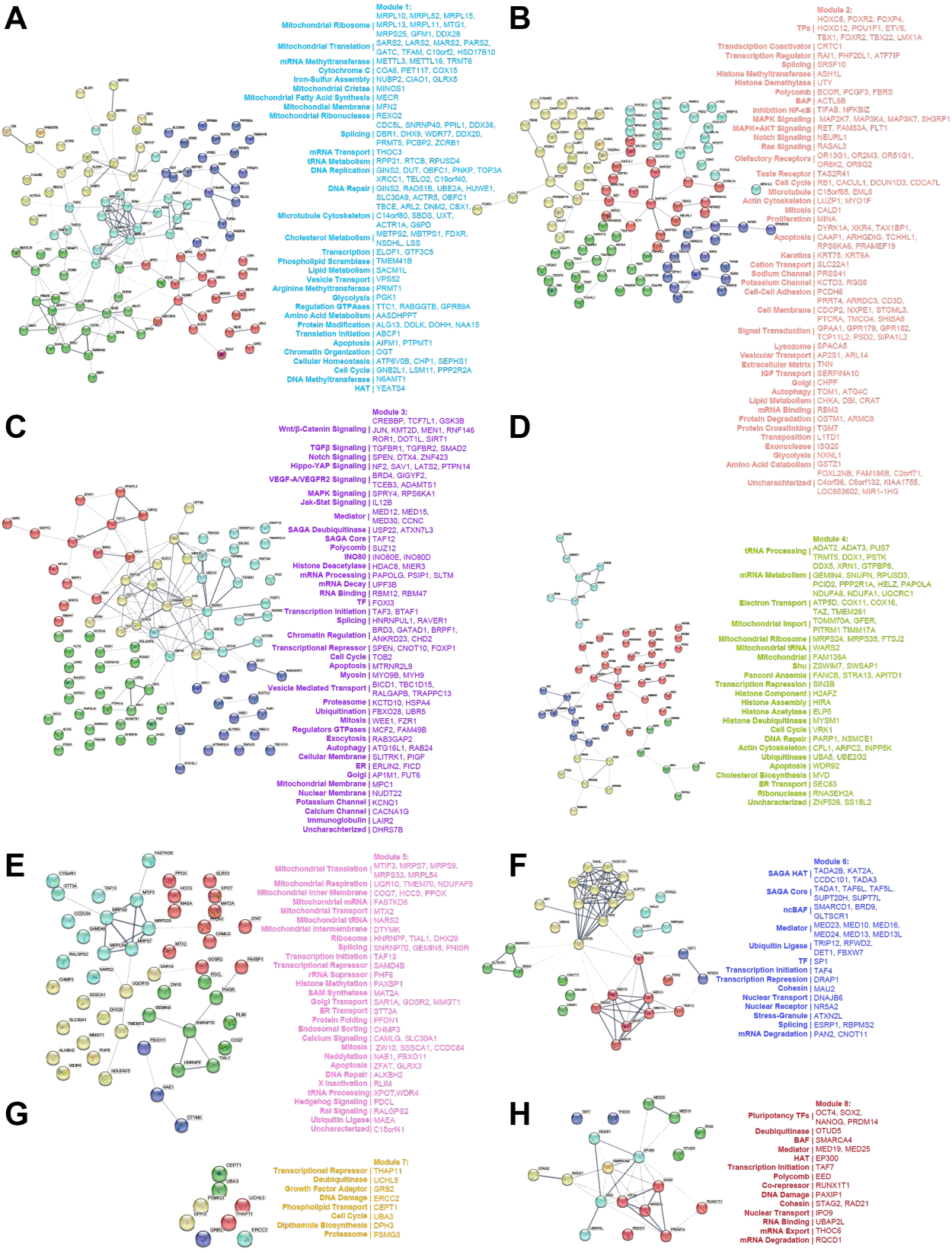
A
Module 1:
Mitochondrial Ribosome | MRPL10, MRPL52, MRPL15, MRPL13, MRPL11, MTG1, MRPS25, GFM1, DDX28
Mitochondrial Translation | SARS2, LARS2, MARS2, PARS2, GATC, TFAM, C10orf2, HSD17B10
mRNA Methyltransferase | METTL3, METTL16, TRMT6
Cytochrome C | COA6, PET117, COX15
Iron-Sulfur Assembly | NUBP2, CIAO1, GLRX5
Mitochondrial Cristae | MINOS1
Mitochondrial Fatty Acid Synthesis | MECR
Mitochondial Membrane | MFN2
Mitochondrial Ribonuclease | REXO2
Splicing | CDC5L, SNRNP40, PPIL1, DDX36, DBR1, DHX9, WDR77, DDX20, PRMT5, PCBP2, ZCRB1
mRNA Transport | THOC3
tRNA Metabolism | RPP21, RTCB, RPUSD4
DNA Replication | GINS2, DUT, OBFC1, PNKP, TOP3A XRCC1, TELO2, C19orf40,
DNA Repair | GINS2, RAD51B, UBE2A, HUWE1, SLC30A9, ACTR5, OBFC1 TBCE, ARL2, DNM2, CBX1,
Microtubule Cytoskeleton | C14orf80, SBDS, UXT, ACTR1A, G6PD
Cholesterol Metabolism | MBTPS2, MBTPS1, FDXR, NSDHL, LSS
Transcription | ELOF1, GTF3C5
Phospholipid Scramblase | TMEM41B
Lipid Metabolism | SACM1L
Vesicle Transport | VPS52
Arginine Methyltransferase | PRMT1
Glycolysis | PGK1
Regulation GTPAses | TTC1, RABGGTB, GPR89A
Amino Acid Metabolism | AASDHPPT
Protein Modification | ALG13, DOLK, DOHH, NAA15
Translation Initiation | ABCF1
Apoptosis | AIFM1, PTPMT1
Chromatin Organization | OGT
Cellular Homeostasis | ATP6V0B, CHP1, SEPHS1
Cell Cycle | GNB2L1, LSM11, PPP2R2A
DNA Methyltransferase | N6AMT1
HAT | YEATS4
B
Module 2:
TFs | HOXC8, FOXR2, FOXP4, HOXC12, POU1F1, ETV6, TBX1, FOXR2, TBX22, LMX1A
Transcription Coactivator | CRTC1
Transcription Regulator | RAI1, PHF20L1, ATF7IP
Splicing | SRSF10
Histone Methyltransferase | ASH1L
Histone Demethylase | UTY
Polycomb | BCOR, PCGF3, FBRS
BAF | ACTL6B
Inhibition NF-κB | TIFAB, NFKBIZ
MAPK Signaling | MAP2K7, MAP3K4, MAP3K7, SH3RF1
MAPK+AKT Signaling | RET, FAM83A, FLT1
Notch Signaling | NEURL1
Ras Signaling | RASAL3
Olefactory Receptors | OR13G1, OR2M3, OR51G1, OR9K2, OR9Q2
Taste Receptor | TAS2R41
Cell Cycle | RB1, CACUL1, DCUN1D3, CDCA7L
Microtubule | C15orf65, EML6
Actin Cytoskeleton | LUZP1, MYO1F
Mitosis | CALD1
Proliferation | MINA
Apoptosis | DYRK1A, XKR4, TAX1BP1, CAAP1, ARHGDIG, TCHHL1, RPS6KA6, PRAMEF19
Keratins | KRT75, KRT6A
Cation Transport | SLC22A1
Sodium Channel | PRSS41
Potassium Channel | KCTD3, RGS8
Cell-Cell Adhesion | PCDH8
Cell Membrane | PRRT4, ARRDC3, CD3D, CDCP2, NXPE1, STOML3, PTCRA, TMCO4, SHISA8
Signal Transduction | GPAA1, GPR179, GPR182, TCP11L2, PSD2, SIPA1L2
Lysozome | SPACA5
Vesicular Transport | AP2S1, ARL14
Extracellular Matrix | TNN
IGF Transport | SERPINA10
Golgi | CHPF
Autophagy | TOM1, ATG4C
Lipid Metabolism | CHKA, DBI, CRAT
mRNA Binding | RBM3
Protein Degradation | OSTM1, ARMC8
Protein Crosslinking | TGM7
Transposition | L1TD1
Exonuclease | ISG20
Glycolysis | NXNL1
Amino Acid Catabolism | GST21
Uncharachterized | FOXL2NB, FAM186B, C2orf71, C4orf36, C6orf132, KIAA1755, LOC653602, MIR1-1HG
C
Module 3:
Wnt/β-Catenin Signaling | CREBBP, TCF7L1, GSK3B JUN, KMT2D, MEN1, RNF146 ROR1, DOT1L, SIRT1
TGFβ Signaling | TGFBR1, TGFBR2, SMAD2
Notch Signaling | SPEN, DTX4, ZNF423
Hippo-YAP Signaling | NF2, SAV1, LATS2, PTPN14
VEGF-A/VEGFR2 Signaling | BRD4, GIGYF2, TCEB3, ADAMTS1
MAPK Signaling | SPRY4, RPS6KA1
Jak-Stat Signaling | IL12B
Mediator | MED12, MED15, MED30, CCNC
SAGA Deubiquitinase | USP22, ATXN7L3
SAGA Core | TAF12
Polycomb | SUZ12
INO80 | INO80E, INO80D
Histone Deacetylase | HDAC8, MIER3
mRNA Processing | PAPOLG, PSIP1, SLTM
mRNA Decay | UPF3B
RNA Binding | RBM12, RBM47
TF | FOXI3
Transcription Initiation | TAF3, BTAF1
Splicing | HNRNPUL1, RAVER1
Chromatin Regulation | BRD3, GATAD1, BRPF1, ANKRD23, CHD2
Transcriptional Repressor | SPEN, CNOT10, FOXP1
Cell Cycle | TOB2
Apoptosis | MTRNR2L9
Myosin | MYO9B, MYH9
Vesicle Mediated Transport | BICD1, TBC1D15, RALGAPB, TRAPPC13
Proteasome | KCTD10, HSPA4
Ubiquitination | FBXO28, UBR5
Mitosis | WEE1, FZR1
Regulators GTPases | MCF2, FAM49B
Exocytosis | RAB3GAP2
Autophagy | ATG16L1, RAB24
Cellular Membrane | SLITRK1, PIGF
ER | ERLIN2, FICD
Golgi | AP1M1, FUT6
Mitochondrial Membrane | MPC1
Nuclear Membrane | NUDT22
Potassium Channel | KCNQ1
Calcium Channel | CACNA1G
Immunoglobulin | LAIR2
Uncharachterized | DHRS7B
D
Module 4:
tRNA Processing | ADAT2, ADAT3, PUS7 TRMT5, DDX1, PSTK
mRNA Metabolism | DDX5, XRN1, GTPBP8, GEMIN4, SNUPN, RPUSD3, PCID2, PPP2R1A, HELZ, PAPOLA
Electron Transport | NDUFA8, NDUFA1, UQCRC1 ATP5D, COX11, COX16,
Mitochondrial Import | TAZ, TMEM261 TOMM70A, GFER, PITRM1 TIMM17A
Mitochondrial Ribosome | MRPS24, MRPS35, FTSJ2
Mitochondrial tRNA | WARS2
Mitochondrial | FAM136A
Shu | ZSWIM7, SWSAP1
Fanconi Anaemia | FANCB, STRA13, APITD1
Transcription Repression | SIN3B
Histone Component | H2AFZ
Histone Assembly | HIRA
Histone Acetylase | ELP5
Histone Deubiquitinase | MYSM1
Cell Cycle | VRK1
DNA Repair | PARP1, NSMCE1
Actin Cytoskeleton | CFL1, ARPC2, INPP5K
Ubiquitinase | UBA5, UBE2G2
Apoptosis | WDR92
Cholesterol Biosynthesis | MVD
ER Transport | SEC63
Ribonuclease | RNASEH2A
Uncharacterized | ZNF526, SS18L2
E
Module 5:
Mitochondrial Translation | MTIF3, MRPS7, MRPS9, MRPS33, MRPL54
Mitochondrial Respiration | UQRC10, TMEM70, NDUFAF5
Mitochondrial Inner Membrane | COQ7, HCCS, PPOX
Mitochondrial mRNA | FASTKD5
Mitochondrial Transport | MTX2
Mitochondrial tRNA | NARS2
Mitochondrial Intermembrane | DTYMK
Ribosome | HNRNPF, TIAL1, DHX29
Splicing | SNRNP70, GEMIN8, PNISR
Transcription Initiation | TAF13
Transcriptional Repressor | SAMD4B
rRNA Supressor | PHF5
Histone Methylation | PAXBP1
SAM Synthetase | MAT2A
Golgi Transport | SAR1A, GOSR2, MMGT1
ER Transport | STT3A
Protein Folding | PFDN1
Endosomal Sorting | CHMP3
Calcium Signaling | CAMLG, SLC30A1
Mitosis | ZW10, SSSCA1, CCDC84
Neddylation | NAE1, FBXO11
Apoptosis | ZFAT, GLRX3
DNA Repair | ALKBH2
X Inactivation | RLIM
tRNA Processing | XPOT,WDR4
Hedgehog Signaling | PDCL
Ras Signaling | RALGPS2
Ubiquitin Ligase | MAEA
Uncharacterized | C15orf41
F
Module 6:
SAGA HAT | TADA2B, KAT2A, CCDC101, TADA3
SAGA Core | TADA1, TAF6L, TAF5L, SUPT20H, SUPT7L
ncBAF | SMARCD1, BRD9, GLTSCR1
Mediator | MED23, MED10, MED16, MED24, MED13, MED13L
Ubiquitin Ligase | TRIP12, RFWD2, DET1, FBXW7
TF | SP1
Transcription Initiation | TAF4
Transcription Repression | DRAP1
Cohesin | MAU2
Nuclear Transport | DNAJB6
Nuclear Receptor | NR5A2
Stress-Granule | ATXN2L
Splicing | ESRP1, RBPMS2
mRNA Degradation | PAN2, CNOT11
G
Module 7:
Transcriptional Repressor | THAP11
Deubiquitinase | UCHL5
Growth Factor Adaptor | GRB2
DNA Damage | ERCC2
Phospholipid Transport | CEPT1
Cell Cycle | UBA3
Dipthamide Biosynthesis | DPH3
Proteasome | PSMG3
H
Module 8:
Pluripotency TFs | OCT4, SOX2, NANOG, PRDM14
Deubiquitinase | OTUD5
BAF | SMARCA4
Mediator | MED19, MED25
HAT | EP300
Transcription Initiation | TAF7
Polycomb | EED
Co-repressor | RUNX1T1
DNA Damage | PAXIP1
Cohesin | STAG2, RAD21
Nuclear Transport | IPO9
RNA Binding | UBAP2L
mRNA Export | THOC6
mRNA Degradation | RQCD1

Figure S7. Distinct gene sets identified in individual modules (A) Interactome indicating known associations between members of cluster gene sets identified through STRING analysis[30] using default parameters for high-confidence interactions. Each gene-set was further clustered using k-means clustering (k=5), and dotted lines indicate connections between clusters. Annotation of all genes in Module 1, (B) Module 2, (C) Module 3, (D), Module 4, (E) Module 5, (F) Module 6, (G) Module 7, and (H) Module 8.

Key Resources and Supplemental Tables

Key resources table

REAGENT or RESOURCE	SOURCE	IDENTIFIER
Antibodies		
eFluor660 conjugated rat anti-human OCT4	eBioscience	Cat# 50-5841-82; RRID:AB_11218882
AlexaFluor488 conjugated rat anti-GFP	Biolegend	Cat# 338008; RRID:AB_2563288
Mouse anti-human TADA2B	Abnova	Cat# H00093624-M08
Rabbit anti-human GAPDH	Cell Signaling Technology	Cat# 5174; RRID:AB_561053
Rabbit anti-human OTUD5	Cell Signaling Technology	Cat# 20087; RRID:AB_2798833
IRDye800 conjugated donkey anti-mouse	LI-COR	Cat# 926-32212
IRDye680 conjugated donkey anti-mouse	LI-COR	Cat# 926-68073
Rabbit anti-human OCT4	Cell Signaling Technology	Cat# 5677; RRID:AB_10547892
Bacterial and virus strains		
One Shot Stbl3a Chemically Competent E. coli	Invitrogen	Cat# C7373-03
Chemicals, peptides, and recombinant proteins		
Essential 8	Thermo Fisher Scientific	Cat# A1517001
Vitronectin	Thermo Fisher Scientific	Cat# A14700
Y-27632	Selleck Chemicals	Cat# S1049
EDTA	KD Medical	Cat# RGE-3130
Lipofectamine 3000	Thermo Fisher Scientific	Cat# L3000001
TrypLE	Thermo Fisher Scientific	Cat# 12563-029
Opti-MEM	Thermo Fisher Scientific	Cat# 31985070
Essential 6	Thermo Fisher Scientific	Cat# A1516401
SB431542	Tocris	Cat# 161410
LDN193189	Cedarlane Labs	Cat# 04-0074-02
MCDB131	Thermo Fisher Scientific	Cat# 10372019
Sodium Bicarbonate	Research Products International	Cat# S22060
Glutamax	Thermo Fisher Scientific	Cat# 35050061
Activin A	Bon-Opus Biosciences	Cat# C687-1mg
CHIR99021	Stemgent	Cat# 04-0004-10
D-glucose	Sigma-Aldrich	Cat# G8769
Bovine Serum Albumin	LAMPIRE	Cat# 7500804

Doxycycline	Thermo Fisher Scientific	Cat# BP26535
Puromycin	Sigma-Aldrich	Cat# P8833
Protamine Sulfate	MP Biomedicals	Cat# 0219472901
RNAiMAX	Thermo Fisher Scientific	Cat# 13778100
Bis-Tris 10% gel	Novex	Cat# NP0301BOX
Nitrocellulose membrane	Novex	Cat# LC2001
Non-Fat Dry Milk	LabScientific	Cat# M-0841
SDS 20% solution	Thermo Fisher Scientific	Cat# AM9820
DTT	Thermo Fisher Scientific	Cat# FERR0861
iodoacetamide	VWR	Cat# IC10035105
Phosphoric acid	Thermo Fisher Scientific	Cat# A2421
Sequencing grade modified trypsin	Promega	Cat# V5111
Critical commercial assays		
TOPO TA Cloning Kit	Thermo Fisher Scientific	Cat# 450641
LIVE-DEAD Fixable Violet Dead Cell Stain	Thermo Fisher Scientific	Cat# L34955
Blood & Cell Culture DNA Maxi Kit	QIAGEN	Cat# 13362
Zero Blunt TOPO PCR Cloning Kit	Thermo Fisher Scientific	Cat# 450245
Zyppy Plasmid Miniprep Kit	Zymo	Cat# D4037
Bradford Protein Assay	Bio-Rad	Cat# 500-0202
S-trap micro columns	Protifi	Cat# C02-micro-80
Experimental models: Cell lines		
H1 hESCs with inducible Cas9	[76]	
HUES8 hESCs with inducible Cas9	[20]	
OCT4-GFP reporter H1 hESCs with inducible Cas9	This study	
TADA2B KOs #1 in HUES8 hESCs with inducible Cas9	This study	
TADA2B KOs #2 in HUES8 hESCs with inducible Cas9	This study	
TADA2B KOs #3 in HUES8 hESCs with inducible Cas9	This study	
OTUD5 KO #1 in HUES8 hESCs with inducible Cas9	This study	
OTUD5 KO #2 in HUES8 hESCs with inducible Cas9	This study	
HEK293T	Laboratory of Robert Weinberg	RRID: CVCL_0063
Oligonucleotides		
Primers for OCT4-GFP line construction, all cell line sequencing, and CRISPR screen gRNA library sequencing, See **Table S5**	This study	
tracrRNA	IDT	Cat# 1072532
gRNAs for validation and KO generation, See **Table S6**	This study	
Recombinant DNA		
pOCT4-2A-copGFP	This study	
lentiGuide-puro	[85]	Addgene,Cat# 52963

pCMV-VSV-G	[86]	Addgene,Cat# 8454
psPAX2	Laboratory of Didier Trono	Addgene,Cat# 12260
pWPXL_Luc2tdT	[87]	
pLARRY Barcode Library Version 1	[89]	Addgene,Cat# 140024
Software and algorithms		
FlowJo v10	BD Biosciences	
R (version 4.1.3)	R Core Team	https://www.r-project.org/
Illustrator	Adobe Ink	
Prism	Graphpad	
MAGeCK 0.5.9.4	[24]	https://sourceforge.net/projects/mageck/
GSEA Software Version 4.2.3	[79,80]	https://www.gsea-msigdb.org/gsea/
UpSetR shiny app	[82,83]	https://gehlenborglab.shinyapps.io/upsetr/
ggplot2 R package	[81]	https://cran.r-project.org/web/packages/ggplot2/
STRING V11.5	[30]	https://string-db.org/
Metascape 3.5	[31]	https://metascape.org/
Reactome-PA R package	[41]	https://bioconductor.org/packages/release/bioc/html/ReactomePA.html
FASTX-Toolkit		http://hannonlab.cshl.edu/fastx_toolkit/
CRISPResso2	[90]	http://crispresso.pinellolab.org/submission
Proteome Discoverer v2.4	Thermo Fisher Scientific	
Cytoscape v3.9.1	[94]	Cytoscape.org
Other		
Vi-CELL XR Cell Viability Analyzer	Beckman Coulter	
LSRFortessa	BD Biosciences	
LSRII	BD Biosciences	
lentiviral packaged genome-scale Brunello gRNA library	[17,95]	
FacsAria	BD Biosciences	
HiSeq 2500	Illumina	
Odyssey DLx Imaging System	LICOR	
Dionex RSLC Ultimate 300	Thermo Fisher Scientific	
Orbitrap Fusion Lumos	Thermo Fisher Scientific	

Table S1. MAGeCK analysis of NE, DE, E8, and E6 screens Sheets 1-4 results from MAGeCK [24] analysis of NE, DE, E8, and E6 screens. Data were analyzed with MAGeCK 0.5.9.4 default RRA parameters. Sheets 5-8 NE, DE, E8, and E6 screen gRNA raw counts.

Table S2. Previous pro-self-renewal and essentiality data sets Sheet 1 gene sets used for GSEA comparison with previous hESC self-renewal screens. Gene sets from previous screens by Yilmaz et al. [11], Mair et al. [12], and Ihry et al. [13], as re-analyzed by Mair et al. using BAGEL analysis [84]. For all self-renewal screens, top 150 pro-self-renewal hits were calculated by highest Bayes Factor for fold change in late time point vs. early timepoint. Sheet 2 common essentiality genes shown are the "CRISPRInferredCommonEssentials" data set from DepMap [43,44,46] version 22Q4 [42].

Table S3. Pro-pluripotency and pro-self-renewal hits by module Top 150 pro-pluripotency and pro-self-renewal hits from NE, DE, E8, and E6 screens by module, z-scores and LFC per gene . Z-scores = column scaled LFC. LFC = Log_2(Fold Change OCT4-GFP^{hi} / OCT4-GFP^{lo}) for NE and DE screens or Log_2(Fold Change Day 0/ Day 10) for E8 and E6 screens.

Table S4. OTUD5 and OCT4 ChIP-MS Sheets 1-2 results from OTUD5 ChIP-MS in NE Day 1 (NED1), and DE Day 1 (DED1). *OTUD5* KO cells stained with OTUD5 antibody was used as a negative control. Sheet 3 results from OCT4 ChIP-MS in hESCs (E8). WT cells stained with IgG was used as a negative control. Sheets 4-6, raw data from OTUD5 and OCT4 ChIP-MS experiments.

Table S5. Related to Key Resources Table: Primers Used for cloning OCT4-GFP reporter, PCR and sequencing of cell lines, and CRISPR screen Hi-Seq

Name	Sequence	Use

NhPTV-F	GCTAGCACCGGTGCCAC GAACTTCTCT	Generation NheI-2A-copGFP-AscI cassette (forward).
Asc_St_copGFP-R	GGCGCGCCTTAGGCGAA GGCGATGGGGGT	Generation NheI-2A-copGFP-AscI cassette (reverse).
AgPTVppGFP-F	ACCGGTGCCACGAACTTC TCTCTGTTAAAGCAAGCA GGAGACGTGGAAGAAAAC CCCGGTCCTATGCCCGCC ATGAAGATCGAG	Generation AgeI-PTV1-2A-ppGFP cassette (forward)
ppGFP-R	TTAGGCGAAGGCGATGG GGGT	Generation AgeI-PTV1-2A-ppGFP cassette (reverse)
OCT4 upstream 5'-F	AGTGGTTCTCAGTGGGAT GG	Amplifying region of OCT4-2A-copGFP insert outside of homology arm (forward).
OCT4 3'_hom-R	ACTTCACCTTCCCTCCAA CC	Amplifying region of OCT4-2A-copGFP insert (reverse).
OCT4 5'_hom-F	CGAGAGGATTTTGAGGCT GC	Amplifying region of OCT4-2A-copGFP insert (forward).
OCT4 downstream 3'-R	ACTAGTGGCAGAGCCAGG AA	Amplifying region of OCT4-2A-copGFP insert outside of homology arm (reverse).
OTUD5 clonal KO seq-F	TTCTGCAGTGGGTAGGTG AG	Amplifying mutated region in *OTUD5* (forward).
OTUD5 clonal KO seq-R	CCCCTGGTTTGAATGATG GC	Amplifying mutated region in *OTUD5* (reverse).
TADA2B clonal KO seq-F	GTGAGCATGTACATCCAC GG	Amplifying mutated region in *TADA2B* (forward).
TADA2B clonal KO seq-R	ATAGTTGACAGAGAGCCC GC	Amplifying mutated region in *TADA2B* (reverse).
LARRY Barcodes-F	GTGGCGATATCGGATCCA	Amplifying LARRY Barcodes, cell competition (forward)
LARRY Barcodes-R	TTGCTAGGAGAGACCATA	Amplifying LARRY Barcodes, cell competition (reverse)
Hi-Seq-first-F	AATGGACTATCATATGCTT ACCGTAACTTGAAAGTATT TCG	CRISPR-screen Hi-Seq first step PCR, matched to sequence lentiGuide-puro (forward)
Hi-Seq-first-R	CTTTAGTTTGTATGTCTGT TGCTATTATGTCTACTATT CTTTC	CRISPR-screen Hi-Seq first step PCR, matched to sequence lentiGuide-puro (reverse)
Hi-Seq-second-F	AATGATACGGCGACCACC GAGATCTACACTCTTTCC CTACACGACGCTCTTC CGATCT(1-9bp variable length sequence)tcttgtggaaaggacga aacaccg	CRISPR-screen Hi-Seq second step PCR, uppercase matched to flowcell attachment, lowercase matched to sequence lentiGuide-puro (forward)
Hi-Seq-second-R	CAAGCAGAAGACGGCATA CGAGAT(8bp barcode)	CRISPR-screen Hi-Seq second step PCR, uppercase

	GTGACTGGAGTTCAGACG TGTGCTCTTCCGATCTtcta ctattctttcccctgcactgt	matched to flowcell attachment, lowercase matched to sequence lentiGuide-puro (reverse)

Table S6. Related to Key Resources Table: List of gRNA Target Sequences Guide RNAs were used for targeting of the *OCT4* locus for creation of the OCT4-GFP reporter line; lentiviral KOs during validation of screening hits; and clonal KO of *OTUD5* or *TADA2B*.

Name	**gRNA Target Sequence**
OCT4_Stp_cRNA	TCTCCCATGCATTCAAACTG
Non-targeting_control #1_lenti	ACGGAGGCTAAGCGTCGCAA
Non-targeting_control #2_lenti	CGCTTCCGCGGCCCGTTCAA
SMARCD1_lenti	TTTGTCCAGTTCAATCACCA
TAF6L_lenti	AGATCCTGGCAGATCCTGTG
TADA2B_lenti	ATCTCGTAATCATCCCGCAG
EP300_lenti	CTGTAATAAGTGGCATCACG
ESRP1_lenti	AATATGCACAGAATGCGTTG
SOX2_lenti	CGTTCATCGACGAGGCTAAG
OTUD5_lenti	CCATTCGTGTTAGCTACCAT
CCDC101_lenti	ACATCCAGAAGACCCATGAG
RFWD2_lenti	TACCAATCTAGACAACTCAG
RBPMS2_lenti	AGGAGCACACTTCATCGCAC
ZNF423_lenti	GGTGCAGTGGTACAACACAA
FBRS_lenti	CTGAGCTGCCACCACGACTG
SLTM_lenti	AAACCTCTTTGCTTGACCAG
HOXC8_lenti	GTGGACGGCAAACTTACAGC
PAPOLG_lenti	AACATGCTAGGATTCCTTGG
RB1_lenti	GGTTCTTTGAGCAACATGGG
CARM1_lenti	TTGAAGAGCATGTAGCCCAT
UBA6_lenti	TTGTAAGACTCAGTCAAATG
DHX36_lenti	ACGTTGGCCAGATTATGTAA
OTUD5_cRNA	CCATTCGTGTTAGCTACCAT
TADA2B_cRNA	ATCTCGTAATCATCCCGCAG

References

1. Nichols, J., Zevnik, B., Anastassiadis, K., Niwa, H., Klewe-Nebenius, D., Chambers, I., Scholer, H., and Smith, A. (1998). Formation of pluripotent stem cells in the mammalian embryo dependes on the POU transcription factor Oct4. Cell *95*, 379–391. 10.1016/S0092-8674(00)81769-9.
2. Niwa, H., Miyazaki, J., and Smith, A.G. (2000). Quantitative expression of Oct-3/4 defines differentiation, dedifferentiation or self-renewal of ES cells. Nat. Genet. *24*, 372–376. 10.1038/74199.
3. Mitsui, K., Tokuzawa, Y., Itoh, H., Segawa, K., Murakami, M., Takahashi, K., Maruyama, M., Maeda, M., and Yamanaka, S. (2003). The homeoprotein Nanog is required for maintenance of pluripotency in mouse epiblast and ES cells. Cell *113*, 631–642. 10.1016/j.cell.2006.07.024.
4. Avilion, A.A., Nicolis, S.K., Pevny, L.H., Perez, L., Vivian, N., and Lovell-Badge, R. (2003). Multipotent cell lineages in early mouse development on SOX2 function. Genes Dev. *17*, 126–140. 10.1101/gad.224503.
5. Chambers, I., Colby, D., Robertson, M., Nichols, J., Lee, S., Tweedie, S., and Smith, A. (2003). Functional expression cloning of Nanog, a pluripotency sustaining factor in embryonic stem cells. Cell *113*, 643–655. 10.1016/S0092-8674(03)00392-1.
6. Boyer, L.A., Lee, T.I., Cole, M.F., Johnstone, S.E., Levine, S.S., Zucker, J.P., Guenther, M.G., Kumar, R.M., Murray, H.L., Jenner, R.G., et al. (2005). Core Transcriptional Regulatory Circuitry in Human Embryonic Stem Cells. Cell *122*, 947–956. 10.1016/j.cell.2005.08.020.
7. Loh, Y.H., Wu, Q., Chew, J.L., Vega, V.B., Zhang, W., Chen, X., Bourque, G., George, J., Leong, B., Liu, J., et al. (2006). The Oct4 and Nanog transcription network regulates pluripotency in mouse embryonic stem cells. Nat. Genet. *38*, 431–440. 10.1038/ng1760.
8. Liu, J.C., Guan, X., Ryan, J.A., Rivera, A.G., Mock, C., Agarwal, V., Letai, A., Lerou, P.H.,

and Lahav, G. (2013). High mitochondrial priming sensitizes hESCs to DNA-damage-induced apoptosis. Cell Stem Cell *13*, 483–491. 10.1016/j.stem.2013.07.018.

9. Naxerova, K., Di Stefano, B., Makofske, J.L., Watson, E. V, de Kort, M.A., Martin, T.D., Dezfulian, M., Ricken, D., Wooten, E.C., Kuroda, M.I., et al. (2021). Integrated loss- and gain-of-function screens define a core network governing human embryonic stem cell behavior. Genes Dev., 1–21. 10.1101/gad.349048.121.

10. Shalem, O., Sanjana, E.N., Hartenian, E., and Zhang, F. (2014). Genome-Scale CRISPR-Cas9 Knockout Screening in Human Cells. Science (80-.). *343*, 84–88. 10.1038/nbt.2647.

11. Yilmaz, A., Peretz, M., Aharony, A., Sagi, I., and Benvenisty, N. (2018). Defining essential genes for human pluripotent stem cells by CRISPR–Cas9 screening in haploid cells. Nat. Cell Biol. 10.1038/s41556-018-0088-1.

12. Mair, B., Tomic, J., Masud, S.N., Tonge, P., Weiss, A., Usaj, M., Tong, A.H.Y., Kwan, J.J., Brown, K.R., Titus, E., et al. (2019). Essential Gene Profiles for Human Pluripotent Stem Cells Identify Uncharacterized Genes and Substrate Dependencies. Cell Rep. *27*, 599-615.e12. 10.1016/j.celrep.2019.02.041.

13. Ihry, R.J., Salick, M.R., Ho, D.J., Sondey, M., Kommineni, S., Paula, S., Raymond, J., Henry, B., Frias, E., Wang, Q., et al. (2019). Genome-Scale CRISPR Screens Identify Human Pluripotency-Specific Genes. Cell Rep. *27*, 616-630.e6. 10.1016/j.celrep.2019.03.043.

14. Li, Q. V., Rosen, B.P., and Huangfu, D. (2020). Decoding pluripotency: Genetic screens to interrogate the acquisition, maintenance, and exit of pluripotency. WIREs Syst. Biol. Med. *12*, 1–25. 10.1002/wsbm.1464.

15. Chambers, S.M., Fasano, C.A., Papapetrou, E.P., Tomishima, M., Sadelain, M., and Studer, L. (2009). Highly efficient neural conversion of human ES and iPS cells by dual inhibition of SMAD signaling. Nat. Biotechnol. *27*, 275–280. 10.1038/nbt.1529.

16. D'Amour, K.A., Agulnick, A.D., Eliazer, S., Kelly, O.G., Kroon, E., and Baetge, E.E. (2005). Efficient differentiation of human embryonic stem cells to definitive endoderm. Nat. Biotechnol. *23*, 1534–1541. 10.1038/nbt1163.

17. Li, Q. V., Dixon, G., Verma, N., Rosen, B.P., Gordillo, M., Luo, R., Xu, C., Wang, Q., Soh, C.-L., Yang, D., et al. (2019). Genome-scale screens identify JNK-JUN signaling as a barrier for pluripotency exit and endoderm differentiation. Nat. Genet. *51*, 999–1010. 10.1038/s41588-019-0408-9.

18. Fogarty, N.M.E., McCarthy, A., Snijders, K.E., Powell, B.E., Kubikova, N., Blakeley, P., Lea, R., Elder, K., Wamaitha, S.E., Kim, D., et al. (2017). Genome editing reveals a role for OCT4 in human embryogenesis. Nature *550*, 67–73. 10.1038/nature24033.

19. Zhu, Z., Verma, N., González, F., Shi, Z.-D., and Huangfu, D. (2015). A CRISPR/Cas-Mediated Selection-free Knockin Strategy in Human Embryonic Stem Cells. Stem Cell Reports *4*, 1103–1111. 10.1016/j.stemcr.2015.04.016.

20. González, F., Zhu, Z., Shi, Z.D., Lelli, K., Verma, N., Li, Q. V., and Huangfu, D. (2014). An iCRISPR platform for rapid, multiplexable, and inducible genome editing in human pluripotent stem cells. Cell Stem Cell *15*, 215–226. 10.1016/j.stem.2014.05.018.

21. Dixon, G., Pan, H., Yang, D., Rosen, B.P., Jashari, T., Verma, N., Pulecio, J., Caspi, I., Lee, K., Stransky, S., et al. (2021). QSER1 protects DNA methylation valleys from de novo methylation. Science (80-.). *372*. 10.1126/science.abd0875.

22. Yang, D., Cho, H., Tayyebi, Z., Shukla, A., Luo, R., Dixon, G., Ursu, V., Stransky, S., Tremmel, D.M., Sackett, S.D., et al. (2022). CRISPR screening uncovers a central requirement for HHEX in pancreatic lineage commitment and plasticity restriction. Nat. Cell Biol. *24*, 1064–1076. 10.1038/s41556-022-00946-4.

23. Doench, J.G., Fusi, N., Sullender, M., Hegde, M., Vaimberg, E.W., Donovan, K.F., Smith, I., Tothova, Z., Wilen, C., Orchard, R., et al. (2016). Optimized sgRNA design to maximize activity and minimize off-target effects of CRISPR-Cas9. Nat. Biotechnol. *34*,

184–191. 10.1038/nbt.3437.

24. Li, W., Xu, H., Xiao, T., Cong, L., Love, M.I., Zhang, F., Irizarry, R.A., Liu, J.S., Brown, M., and Liu, X.S. (2014). MAGeCK enables robust identification of essential genes from genome-scale CRISPR/Cas9 knockout screens. Genome Biol. *15*, 554. 10.1186/s13059-014-0554-4.

25. Bergsland, M., Werme, M., Malewicz, M., Perlmann, T., and Muhr, J. (2006). The establishment of neuronal properties is controlled by Sox4 and Sox11. Genes Dev. *20*, 3475–3486. 10.1101/gad.403406.

26. Hoodless, P.A., Pye, M., Chazaud, C., Labbé, E., Attisano, L., Rossant, J., and Wrana, J.L. (2001). FoxH1 (Fast) functions to specify the anterior primitive streak in the mouse. Genes Dev. *15*, 1257–1271. 10.1101/gad.881501.

27. Tremblay, K.D., Hoodless, P.A., Bikoff, E.K., and Robertson, E.J. (2000). Formation of the definitive endoderm in mouse is a Smad2-dependent process. Development *127*, 3079–3090. 10.1242/dev.127.14.3079.

28. Sirard, C., De La Pompa, J.L., Elia, A., Itie, A., Mirtsos, C., Cheung, A., Hahn, S., Wakeham, A., Schwartz, L., Kern, S.E., et al. (1998). The tumor suppressor gene Smad4/Dpc4 is required for gastrulation and later for anterior development of the mouse embryo. Genes Dev. *12*, 107–119. 10.1101/gad.12.1.107.

29. Arnold, S.J., Hofmann, U.K., Bikoff, E.K., and Robertson, E.J. (2008). Pivotal roles for eomesodermin during axis formation,epithelium-to-mesenchyme transition and endoderm specification in the mouse. Development *135*, 501–511. 10.1242/dev.014357.

30. Szklarczyk, D., Gable, A.L., Lyon, D., Junge, A., Wyder, S., Huerta-Cepas, J., Simonovic, M., Doncheva, N.T., Morris, J.H., Bork, P., et al. (2019). STRING v11: Protein-protein association networks with increased coverage, supporting functional discovery in genome-wide experimental datasets. Nucleic Acids Res. *47*, D607–D613. 10.1093/nar/gky1131.

31. Zhou, Y., Zhou, B., Pache, L., Chang, M., Khodabakhshi, A.H., Tanaseichuk, O., Benner, C., and Chanda, S.K. (2019). Metascape provides a biologist-oriented resource for the analysis of systems-level datasets. Nat. Commun. *10*. 10.1038/s41467-019-09234-6.

32. Chen, G., Gulbranson, D.R., Hou, Z., Bolin, J.M., Probasco, M.D., Smuga-otto, K., Howden, S.E., Nicole, R., Propson, N.E., Wagner, R., et al. (2011). Chemically defined conditions for human iPS cell derivation and culture. Nat. Methods *8*, 424–429. 10.1038/nmeth.1593.Chemically.

33. Hirsch, C.L., Akdemir, Z.C., Wang, L., Jayakumaran, G., Trcka, D., Weiss, A., Hernandez, J.J., Pan, Q., Han, H., Xu, X., et al. (2015). Myc and SAGA rewire an alternative splicing network during early somatic cell reprogramming. Genes Dev. *29*, 803–816. 10.1101/gad.255109.114.

34. Seruggia, D., Oti, M., Tripathi, P., Canver, M.C., LeBlanc, L., Di Giammartino, D.C., Bullen, M.J., Nefzger, C.M., Sun, Y.B.Y., Farouni, R., et al. (2019). TAF5L and TAF6L Maintain Self-Renewal of Embryonic Stem Cells via the MYC Regulatory Network. Mol. Cell, 1–16. 10.1016/j.molcel.2019.03.025.

35. Papadopoulou, T., Kaymak, A., Sayols, S., and Richly, H. (2016). Dual role of Med12 in PRC1-dependent gene repression and ncRNA-mediated transcriptional activation. Cell Cycle *15*, 1479–1493. 10.1080/15384101.2016.1175797.

36. Chia, N.-Y., Chan, Y.-S., Feng, B., Lu, X., Orlov, Y.L., Moreau, D., Kumar, P., Yang, L., Jiang, J., Lau, M.-S., et al. (2010). A genome-wide RNAi screen reveals determinants of human embryonic stem cell identity. Nature *468*, 316–320. 10.1038/nature09531.

37. Ho, L., Ronan, J.L., Wu, J., Staahl, B.T., Chen, L., Kuo, A., Lessard, J., Nesvizhskii, A.I., Ranish, J., and Crabtree, G.R. (2009). An embryonic stem cell chromatin remodeling complex, esBAF, is essential for embryonic stem cell self-renewal and pluripotency. Proc. Natl. Acad. Sci. U. S. A. *106*, 5181–5186. 10.1073/pnas.0812889106.

38. Kidder, B.L., Palmer, S., and Knott, J.G. (2009). SWI/SNF-Brg1 regulates self-renewal

and occupies core pluripotency-related genes in embryonic stem cells. Stem Cells *27*, 317–328. 10.1634/stemcells.2008-0710.

39. Zhang, X., Li, B., Li, W., Ma, L., Zheng, D., Li, L., Yang, W., Chu, M., Chen, W., Mailman, R.B., et al. (2014). Transcriptional Repression by the BRG1-SWI/SNF Complex Affects the Pluripotency of Human Embryonic Stem Cells. Stem Cell Reports *3*, 460–474. 10.1016/j.stemcr.2014.07.004.

40. Huang, X., Park, K. mi, Gontarz, P., Zhang, B., Pan, J., McKenzie, Z., Fischer, L.A., Dong, C., Dietmann, S., Xing, X., et al. (2021). OCT4 cooperates with distinct ATP-dependent chromatin remodelers in naïve and primed pluripotent states in human. Nat. Commun. *12*. 10.1038/s41467-021-25107-3.

41. Yu, G., and He, Q.-Y. (2016). ReactomePA: an R/Bioconductor package for reactome pathway analysis and visualization. Mol. BioSyst. *12*, 477–479. 10.1039/C5MB00663E.

42. DepMap; Broad (2022). No Title. figshare. Dataset *DepMap 22Q*. doi.org/10.6084/m9.figshare.21637199.v2.

43. Meyers, R.M., Bryan, J.G., Mcfarland, J.M., Weir, B.A., Sizemore, A.E., Xu, H., Dharia, N. V, Montgomery, P.G., Cowley, G.S., Pantel, S., et al. (2017). Computational correction of copy number effect improves specificity of CRISPR – Cas9 essentiality screens in cancer cells. *49*. 10.1038/ng.3984.

44. Dempster, J.M., Rossen, J., Kazachkova, M., Pan, J., Kugener, G., Root, D.E., and Tsherniak, A. (2019). Extracting Biological Insights from the Project Achilles Genome-Scale CRISPR Screens in Cancer Cell Lines. bioRxiv. 10.1101/720243.

45. Dempster, J.M., Boyle, I., Vazquez, F., Root, D., Boehm, J.S., Hahn, W.C., Tsherniak, A., and McFarland, J.M. (2021). Chronos: a CRISPR cell population dynamics model. bioRxiv, 2021.02.25.432728.

46. Pacini, C., Dempster, J.M., Boyle, I., Gonçalves, E., Najgebauer, H., Karakoc, E., van der Meer, D., Barthorpe, A., Lightfoot, H., Jaaks, P., et al. (2021). Integrated cross-study

datasets of genetic dependencies in cancer. Nat. Commun. *12*, 1–14. 10.1038/s41467-021-21898-7.

47. Mashtalir, N., D'Avino, A.R., Michel, B.C., Luo, J., Pan, J., Otto, J.E., Zullow, H.J., McKenzie, Z.M., Kubiak, R.L., St. Pierre, R., et al. (2018). Modular Organization and Assembly of SWI/SNF Family Chromatin Remodeling Complexes. Cell *175*, 1272-1288.e20. 10.1016/j.cell.2018.09.032.

48. Gatchalian, J., Malik, S., Ho, J., Lee, D.S., Kelso, T.W.R., Shokhirev, M.N., Dixon, J.R., and Hargreaves, D.C. (2018). A non-canonical BRD9-containing BAF chromatin remodeling complex regulates naive pluripotency in mouse embryonic stem cells. Nat. Commun. *9*. 10.1038/s41467-018-07528-9.

49. Yamaji, M., Ueda, J., Hayashi, K., Ohta, H., Yabuta, Y., Kurimoto, K., Nakato, R., Yamada, Y., Shirahige, K., and Saitou, M. (2013). PRDM14 ensures naive pluripotency through dual regulation of signaling and epigenetic pathways in mouse embryonic stem cells. Cell Stem Cell *12*, 368–382. 10.1016/j.stem.2012.12.012.

50. Seki, Y. (2018). PRDM14 Is a Unique Epigenetic Regulator Stabilizing Transcriptional Networks for Pluripotency. Front. Cell Dev. Biol. *6*, 10–14. 10.3389/fcell.2018.00012.

51. Wang, W.P., Tzeng, T.Y., Wang, J.Y., Lee, D.C., Lin, Y.H., Wu, P.C., Chen, Y.P., Chiu, I.M., and Chi, Y.H. (2012). The EP300, KDM5A, KDM6A and KDM6B Chromatin Regulators Cooperate with KLF4 in the Transcriptional Activation of POU5F1. PLoS One *7*. 10.1371/journal.pone.0052556.

52. Shan, Y., Liang, Z., Xing, Q., Zhang, T., Wang, B., Tian, S., Huang, W., Zhang, Y., Yao, J., Zhu, Y., et al. (2017). PRC2 specifies ectoderm lineages and maintains pluripotency in primed but not naïve ESCs. Nat. Commun. *8*. 10.1038/s41467-017-00668-4.

53. Michel, B.C., D'Avino, A.R., Cassel, S.H., Mashtalir, N., McKenzie, Z.M., McBride, M.J., Valencia, A.M., Zhou, Q., Bocker, M., Soares, L.M.M., et al. (2018). A non-canonical SWI/SNF complex is a synthetic lethal target in cancers driven by BAF complex

perturbation. Nat. Cell Biol. *20*, 1410–1420. 10.1038/s41556-018-0221-1.

54. Kayagaki, N., Phung, Q., Chan, S., Chaudhari, R., Quan, C., O'Rourke, K.M., Eby, M., Pietras, E., Cheng, G., Bazan, J.F., et al. (2007). DUBA: A deubiquitinase that regulates type I interferon production. Science (80-.). *318*, 1628–1632. 10.1126/science.1145918.

55. Huang, O.W., Ma, X., Yin, J., Flinders, J., Maurer, T., Kayagaki, N., Phung, Q., Bosanac, I., Arnott, D., Dixit, V.M., et al. (2012). Phosphorylation-dependent activity of the deubiquitinase DUBA. Nat. Struct. Mol. Biol. *19*, 171–176. 10.1038/nsmb.2206.

56. De Vivo, A., Sanchez, A., Yegres, J., Kim, J., Emly, S., and Kee, Y. (2019). The OTUD5-UBR5 complex regulates FACT-mediated transcription at damaged chromatin. Nucleic Acids Res. *47*, 729–746. 10.1093/nar/gky1219.

57. Beck, D.B., Basar, M.A., Asmar, A.J., Thompson, J.J., Oda, H., Uehara, D.T., Saida, K., Pajusalu, S., Talvik, I., D'Souza, P., et al. (2021). Linkage-specific deubiquitylation by OTUD5 defines an embryonic pathway intolerant to genomic variation. Sci. Adv. *7*, 1–20. 10.1126/sciadv.abe2116.

58. Cox, B.J., Vollmer, M., Tamplin, O., Lu, M., Biechele, S., Gertsenstein, M., Campenhout, C. Van, Floss, T., and Ku, R. (2010). Phenotypic annotation of the mouse X chromosome. 1154–1164. 10.1101/gr.105106.110.1154.

59. Evans, M.J., and Kaufman, M.H. (1981). Establishment in culture of pluripotential cells from mouse embryos. Nature *292*, 154–156.

60. Martin, G.R. (1981). Isolation of a pluripotent cell line from early mouse embryos cultured in medium conditioned by teratocarcinoma stem cells. Proc. Natl. Acad. Sci. *78*, 7634–7638. 10.1073/pnas.78.12.7634.

61. Thomson, J.A., Itskovitz-eldor, J., Shapiro, S.S., Waknitz, M.A., Swiergiel, J.J., Marshall, V.S., and Jones, J.M. (1998). Embryonic Stem Cell Lines Derived from Human Blastocysts. Science (80-.). *282*, 1145–1148.

62. Takahashi, K., and Yamanaka, S. (2006). Induction of Pluripotent Stem Cells from Mouse

Embryonic and Adult Fibroblast Cultures by Defined Factors. *2*, 663–676. 10.1016/j.cell.2006.07.024.

63. Takahashi, K., Tanabe, K., Ohnuki, M., Narita, M., Ichisaka, T., Tomoda, K., and Yamanaka, S. (2007). Induction of pluripotent stem cells from adult human fibroblasts by defined factors. Cell *131*, 861–872. 10.1016/j.cell.2007.11.019.

64. Loh, K.M., and Lim, B. (2011). A precarious balance: Pluripotency factors as lineage specifiers. Cell Stem Cell *8*, 363–369. 10.1016/j.stem.2011.03.013.

65. Gökbuget, D., and Blelloch, R. (2019). Epigenetic control of transcriptional regulation in pluripotency and early differentiation. Dev. *146*. 10.1242/dev.164772.

66. Yang, C.S., Chang, K.Y., and Rana, T.M. (2014). Genome-wide Functional Analysis Reveals Factors Needed at the Transition Steps of Induced Reprogramming. Cell Rep. *8*, 327–337. 10.1016/j.celrep.2014.07.002.

67. Toh, C.X.D., Chan, J.W., Chong, Z.S., Wang, H.F., Guo, H.C., Satapathy, S., Ma, D., Goh, G.Y.L., Khattar, E., Yang, L., et al. (2016). RNAi Reveals Phase-Specific Global Regulators of Human Somatic Cell Reprogramming. Cell Rep. *15*, 2597–2607. 10.1016/j.celrep.2016.05.049.

68. Adamson, B., Norman, T.M., Jost, M., Cho, M.Y., Nuñez, J.K., Chen, Y., Villalta, J.E., Gilbert, L.A., Horlbeck, M.A., Hein, M.Y., et al. (2016). A Multiplexed Single-Cell CRISPR Screening Platform Enables Systematic Dissection of the Unfolded Protein Response. Cell *167*, 1867-1882.e21. 10.1016/j.cell.2016.11.048.

69. Dixit, A., Parnas, O., Li, B., Chen, J., Fulco, C.P., Jerby-Arnon, L., Marjanovic, N.D., Dionne, D., Burks, T., Raychowdhury, R., et al. (2016). Perturb-Seq: Dissecting Molecular Circuits with Scalable Single-Cell RNA Profiling of Pooled Genetic Screens. Cell *167*, 1853-1866.e17. 10.1016/j.cell.2016.11.038.

70. Jaitin, D.A., Weiner, A., Yofe, I., Lara-Astiaso, D., Keren-Shaul, H., David, E., Salame, T.M., Tanay, A., van Oudenaarden, A., and Amit, I. (2016). Dissecting Immune Circuits

by Linking CRISPR-Pooled Screens with Single-Cell RNA-Seq. Cell *167*, 1883-1896.e15. 10.1016/j.cell.2016.11.039.

71. Datlinger, P., Rendeiro, A.F., Schmidl, C., Krausgruber, T., Traxler, P., Klughammer, J., Schuster, L.C., Kuchler, A., Alpar, D., and Bock, C. (2017). Pooled CRISPR screening with single-cell transcriptome readout. Nat. Methods *14*, 297–301. 10.1038/nmeth.4177.

72. Beer, M.A., Shigaki, D., and Huangfu, D. (2020). Enhancer Predictions and Genome-Wide Regulatory Circuits. Annu. Rev. Genomics Hum. Genet. *21*, 37–54. 10.1146/annurev-genom-121719-010946.

73. Sahu, B., Pihlajamaa, P., Zhang, K., Palin, K., Ahonen, S., Cervera, A., Ristimäki, A., Aaltonen, L.A., Hautaniemi, S., and Taipale, J. (2021). Human cell transformation by combined lineage conversion and oncogene expression. Oncogene *40*, 5533–5547. 10.1038/s41388-021-01940-0.

74. Yilmaz, A., and Benvenisty, N. (2019). Defining Human Pluripotency. Cell Stem Cell *25*, 9–22. 10.1016/j.stem.2019.06.010.

75. Kirschner, K., Chandra, T., Kiselev, V., Flores-Santa Cruz, D., Macaulay, I.C., Park, H.J., Li, J., Kent, D.G., Kumar, R., Pask, D.C., et al. (2017). Proliferation Drives Aging-Related Functional Decline in a Subpopulation of the Hematopoietic Stem Cell Compartment. Cell Rep. *19*, 1503–1511. 10.1016/j.celrep.2017.04.074.

76. Shi, Z.D., Lee, K., Yang, D., Amin, S., Verma, N., Li, Q. V., Zhu, Z., Soh, C.L., Kumar, R., Evans, T., et al. (2017). Genome Editing in hPSCs Reveals GATA6 Haploinsufficiency and a Genetic Interaction with GATA4 in Human Pancreatic Development. Cell Stem Cell *20*, 675-688.e6. 10.1016/j.stem.2017.01.001.

77. Tchieu, J., Zimmer, B., Fattahi, F., Amin, S., Zeltner, N., Chen, S., and Studer, L. (2017). A Modular Platform for Differentiation of Human PSCs into All Major Ectodermal Lineages. Cell Stem Cell *21*, 399-410.e7. 10.1016/j.stem.2017.08.015.

78. Rezania, A., Bruin, J.E., Arora, P., Rubin, A., Batushansky, I., Asadi, A., O'Dwyer, S.,

Quiskamp, N., Mojibian, M., Albrecht, T., et al. (2014). Reversal of diabetes with insulin-producing cells derived in vitro from human pluripotent stem cells. Nat Biotechnol *32*, 1121–1133. 10.1038/nbt.3033.

79. Mootha, V.K., Lindgren, C.M., Eriksson, K.-F., Subramanian, A., Sihag, S., Lehar, J., Puigserver, P., Carlsson, E., Ridderstråle, M., Laurila, E., et al. (2003). PGC-1α-responsive genes involved in oxidative phosphorylation are coordinately downregulated in human diabetes. Nat. Genet. *34*, 267–273. 10.1038/ng1180.

80. Subramanian, A., Tamayo, P., Mootha, V.K., Mukherjee, S., Ebert, B.L., Gillette, M.A., Paulovich, A., Pomeroy, S.L., Golub, T.R., Lander, E.S., et al. (2005). Gene set enrichment analysis: A knowledge-based approach for interpreting genome-wide expression profiles. Proc. Natl. Acad. Sci. U. S. A. *102*, 15545–15550. 10.1073/pnas.0506580102.

81. Wickham, H. (2016). ggplot2: Elegant Graphics for Data Analysis (Springer-Verlag New York).

82. Lex, A., Gehlenborg, N., Strobelt, H., Vuillemot, R., and Pfister, H. (2014). UpSet: Visualization of intersecting sets. IEEE Trans. Vis. Comput. Graph. *20*, 1983–1992. 10.1109/TVCG.2014.2346248.

83. Conway, J.R., Lex, A., and Gehlenborg, N. (2017). UpSetR: An R package for the visualization of intersecting sets and their properties. Bioinformatics *33*, 2938–2940. 10.1093/bioinformatics/btx364.

84. Hart, T., and Moffat, J. (2016). BAGEL: A computational framework for identifying essential genes from pooled library screens. BMC Bioinformatics *17*, 1–7. 10.1186/s12859-016-1015-8.

85. Sanjana, N.E., Shalem, O., and Zhang, F. (2014). Improved vectors and genome-wide libraries for CRISPR screening. Nat. Methods *11*, 783–784. 10.1038/nmeth.3047.

86. Stewart, S.A., Dykxhoorn, D.M., Palliser, D., Mizuno, H., Yu, E.Y., An, D.S., Sabatini,

D.M., Chen, I.S.Y., Hahn, W.C., Sharp, P.A., et al. (2003). Lentivirus-delivered stable gene silencing by RNAi in primary cells. RNA *9*, 493–501. 10.1261/rna.2192803.

87. Zhang, Z., Christin, J.R., Wang, C., Ge, K., Oktay, M.H., and Guo, W. (2016). Mammary-Stem-Cell-Based Somatic Mouse Models Reveal Breast Cancer Drivers Causing Cell Fate Dysregulation. Cell Rep. *16*, 3146–3156. 10.1016/j.celrep.2016.08.048.

88. Pulecio, J., Verma, N., Mejía-Ramírez, E., Huangfu, D., and Raya, A. (2017). CRISPR/Cas9-Based Engineering of the Epigenome. Cell Stem Cell *21*, 431–447. 10.1016/j.stem.2017.09.006.

89. Weinreb, C., and , Alejo Rodriguez-Fraticelli, Fernando D. Camargo, A.M.K. (2020). State To Fate During Differentiation. Science (80-.). *367*, 755. 10.1126/science.aaw3381.Weinreb.

90. Clement, K., Rees, H., Canver, M.C., Gehrke, J.M., Farouni, R., Hsu, J.Y., Cole, M.A., Liu, D.R., Joung, J.K., Bauer, D.E., et al. (2019). CRISPResso2 provides accurate and rapid genome editing sequence analysis. Nat. Biotechnol. *37*, 224–226. 10.1038/s41587-019-0032-3.

91. Lee, K., Cho, H., Rickert, R.W., Li, Q. V., Pulecio, J., Leslie, C.S., and Huangfu, D. (2019). FOXA2 Is Required for Enhancer Priming during Pancreatic Differentiation. Cell Rep. *28*, 382-393.e7. 10.1016/j.celrep.2019.06.034.

92. Aguilan, J.T., Kulej, K., and Sidoli, S. (2020). Guide for protein fold change and p-value calculation for non-experts in proteomics. Mol. Omi. *16*, 573–582. 10.1039/D0MO00087F.

93. Tsherniak, A., Vazquez, F., Montgomery, P.G., Weir, B.A., Kryukov, G., Cowley, G.S., Gill, S., Harrington, W.F., Pantel, S., Krill-Burger, J.M., et al. (2017). Defining a Cancer Dependency Map. Cell *170*, 564-576.e16. 10.1016/j.cell.2017.06.010.

94. Shannon, P., Markiel, A., Ozier, O., Baliga, N.S., Wang, J.T., Ramage, D., Amin, N., Schwikowski, B., and Ideker, T. (2003). Cytoscape: A Software Environment for Integrated Models of Biomolecular Interaction Networks. Genome Res. *13*, 2498–2504.

10.1101/gr.1239303.

95. Doench, J.G., Hartenian, E., Graham, D.B., Tothova, Z., Hegde, M., Smith, I., Sullender, M., Ebert, B.L., Xavier, R.J., and Root, D.E. (2014). Rational design of highly active sgRNAs for CRISPR-Cas9-mediated gene inactivation. Nat. Biotechnol. *32*, 1262–1267. 10.1038/nbt.3026.